THE HONG KONG
POLYTECHNIC UNIVERSITY
香港理工大學
Pao Yue-kong Library
包玉剛圖書館

Copyright Undertaking

This thesis is protected by copyright, with all rights reserved.

By reading and using the thesis, the reader understands and agrees to the following terms:

1. The reader will abide by the rules and legal ordinances governing copyright regarding the use of the thesis.

2. The reader will use the thesis for the purpose of research or private study only and not for distribution or further reproduction or any other purpose.

3. The reader agrees to indemnify and hold the University harmless from and against any loss, damage, cost, liability or expenses arising from copyright infringement or unauthorized usage.

FABRICATION OF FLEXIBLE ELECTRODES

FOR PHOTOVOLTAIC APPLICATIONS

WONG CHIU PO

M.Phil

The Hong Kong Polytechnic University

2012

DEPARTMENT OF APPLIED PHYSICS

FABRICATION OF FLEXIBLE ELECTRODES
FOR PHOTOVOLTAIC APPLICATIONS

WONG CHIU PO

A THESIS SUBMITTED IN PARTIAL FULFILLMENT

OF THE REQUIREMENTS FOR THE DEGREE OF

MASTER OF PHILOSOPHY

August 2011

CERTIFICATION OF ORIGINALITY

I hereby declare that this thesis is my own work and that, to the best of my knowledge and belief, it reproduces no material previously published or written nor material that has been accepted for the award of any other degree or diploma, except where due acknowledgement has been made in the text.

_____ (Signed)

___WONG Chiu Po____ (Name of student)

ABSTRACT

Traditional solar cells are usually bulky in size, heavy in weight and expensive in production cost. Because of these constraints, they are impossible for fashion clothing applications. Metalized polymers are new hybrid materials which have already generated a steady research interest because of their high conductivity, high flexibility, light weight and cheap production cost in the application of electronic components. Metalized polyester fibres enhance applicability of these metalized polymers because of their advantageous flexibility and wearability. They provide chances for photovoltaic applications on textile and clothing industry. In the future, solar cell will be fabricated on these plastic fibres so as to develop "wearable solar cell".

The polyester fibres to be metallized in this project were PET fibres whose diameter was around 125 microns. In the first part of this project, the bottom electrodes, the metal coatings on PET fibres which acted as the flexible substrates, were required to have good conductivity. Metallization methods based on wet chemical techniques were used to coat the required metal layers on the plastic fibres. In this project, two different metals (nickel and copper) had been employed. The Ni-coated polyester fibres were fabricated by electroless plating method. The thickness of the Ni-layer was about 200 nanometres. Cu layers with thicknesses

varied from 1.5 to 20 microns were further deposited on the Ni-coated polyester fibres using electro-plating method. The effects of various processing parameters such as sodium hydroxide etching time, concentration of NaOH, deposition time and temperature for the Ni-electroless plating process on the surface roughness of the metal coatings were conducted. The transport properties of the coated metal layers coated were investigated by measuring the current-voltage curve (I-V Curve) using a four-point probe. Based on these measurements, the resistivity as well as conductivity of the metal layers had been worked out. For the structural characterization, surface and cross-sectional morphologies of Ni- and Cu-coated polyester fibres were observed by optical microscope (OM) and scanning electron microscope (SEM). The structural phases of the metal coatings on the polyester fibres were studied by X-ray diffraction (XRD).

In the second part, vertical-aligned ZnO nanorod arrays were grown on Ni-coated polyester fibres by wet chemical methods. ZnO nanorods with length about 2 microns and diameter about 0.5 micron (aspect ratio in between three and four) were deposited onto these Ni-coated polyester fibres using a chemical solution deposition (CBD) technique. Besides direct growth of ZnO nanorods on Ni-coated PET fibres using CBD method, a ZnO seed layer was first deposited on the Ni-coated PET fibres before using the CBD method to coat ZnO nanorod. This ZnO seed layer improved

the vertical alignment of the ZnO nanorods on the metal-coated polyester fibres. This ZnO seed layer was deposited by pulsed laser deposition (PLD). The phases of the grown ZnO nanorods were studied by XRD and Raman spectroscopy. The surface and cross-section morphologies of the ZnO nanorods were examined using field-emission scanning electron microscope (FE-SEM). The optical properties of the ZnO nanorods grown on PET sheet using CBD with same conditions as those on the Ni-coated fibres were also characterized. Room-temperature transmittance measurement and photoluminescence measurement were performed using UV-Visible spectrophotometer and Nd:YAG laser operated with wavelength of 266 nanometre respectively. On the basis of our results, high-quality ZnO nanorods were shown to be successfully fabricated on Ni-coated polyester fibres.

LIST OF PUBLICATIONS

Journal Paper

1. C. P. Wong, C. L. Mak, "Fabrication and characterization of ZnO nanorod arrays grown on nickel-coated polyester fiber," *Advanced Materials Research*, vol. 385, pp. 463-464, 2012.

Conference Paper

1. C. P. Wong, C. L. Mak, "Fabrication and characterization of ZnO nanorod arrays grown on nickel-coated polyester fiber," *Proceeding of International Conference on Advanced Material Research (ICAMR)*, January 2012.

ACKNOWLEDGEMENTS

TABLE OF CONTENT

CHAPTER 1   INTRODUCTION

1.1   General introduction

1.1.1   Flexible electronics

Flexible can mean many qualities: bendable, conformally shaped, elastic, lightweight, nonbreakable, roll-to-roll manufacturable, or large-area. The first flexible electronics is generally recognized as $100\,\mu$m-thick single crystal silicon wafer solar cells fabricated on a plastic substrate in 1960s in order to raise the power to weight ratio for extra-terrestrial satellites use.[1] Today, for industrial community, flexible electronics refer to flexible displays and X-ray sensor arrays; whereas for researchers, flexible electronics mean electronic textiles, displays and sensors of conformal shape, and electronic skin. Among these flexible electronics, electronic textiles are attracted to many researchers because electronic textiles are the perfect match of fashion and manufacturing industries. In this project, flexible electrodes for photovoltaic application are aimed to be fabricated and corresponding device structures are also introduced.

1.1.2　Three generations of solar cell

The word photovoltaic (PV) is composed of two pieces, where "photo" indicates light, and "voltaic" implies that a potential difference (measured in volts) is set up by the action of the light. PV technology is one of the most popular and promising renewable energy resources and simply expressed as converting natural solar energy directly to useful electricity energy. The technology is an ideal solution to solve future energy crisis and relieve global warming problem. Hence, there is great potential for PV technology to be developed in commercial market which has been attracting many researchers to conduct extensive researches in this field.

The development of solar cell has been divided into three generations.[2] In 2003, most solar cells in the market were made up of silicon wafers which are so-called "first generation" technology. This technology has matured and material cost was the most dominate factor which accounted for over 70% of total manufacturing costs. The materials used were mostly silicon wafers with covers made of strengthened glass. There was little potential to reduce the costs. As a result, it had high areal production cost per area (in US/m^2) and moderate efficiency.

"Second generation" of thin film cell technology has begun since the early 1980s. Instead of using silicon wafer as PV cells, thin silicon films have been employed. Thin films resulted in a major advantage to reduce material costs. Thin film cell

technology also has other advantage, it increases the surface area of manufacturing unit. The material used in producing silicon wafer with surface area of 100 cm^2 can be used to produce thin silicon films on glass with surface area of 1 m^2. Even though its production cost per unit area is relatively low, the efficiency is also low. As "second generation" technology matures, cost of the constitution materials, and hence electricity generation cost will become dominate factor again. The devices are required to have thirty-years operating life to balance the costs.

An alternative approach to improve the performance of PV cells is by increasing power conversion efficiency substantially. The theoretical Carnot limit on the conversion of sunlight to electricity is 95% as opposed to the upper limit of 31% for a single junction solar cell under same basis. This suggests that the performance of solar cells could be improved two to three times if different underlying concepts were applied. This approach activates the development of the "third generation" high-performance, low-cost photovoltaic devices. As a result, the "third generation" photovoltaics, using less expensive materials and new technologies, are attracting more and more interest. They are very different from the other two generations which may not rely on a traditional p-n junction to separate photogenerated charge carriers. There are many new concepts such as tandem cell approach and thermophotonic conversion to be introduced and developed in the next decades. The typical examples

of the "third generation" technology are polymer solar cells and hybrid inorganic-organic solar cells such as hybrid nanorod-polymer solar cells.

1.1.3 Substrates for photovoltaic devices

Generally, the most common active layers for the first and second generations' cells are flat and rigid silicon wafer with glass sheet as substrates. The "third generation" is the turning point for developing flexible solar cells on flexible substrates which can dramatically reduce production costs and be made into variety of shapes which broaden the real applications, in particular, the textile industrial applications. Traditional solar cells are bulky in size, heavy in weight and expensive in production cost which is impossible to be applied for fashion clothing. Hence, the "third generation" photovoltaic technologies together with electronic textiles, typically flexible solar cells, could make a great impact on the development of smart textile industry.

1.1.4 Flexible electrodes - metalized plastics

For all electronic devices, regardless of material, function, size and shape, conducting electrodes are necessary requirement. To fabricate flexible solar cell of bendable structure, light weight and large area, organic polymer (plastic) is absolutely

the most promising candidate as flexible substrates. However, most of the plastic substrates are not conductive. Hence, fabricating flexible electrodes of excellent conductivity, adhesion and uniformity on these plastic substrates are hard challenge to researchers.

Metalized plastics are hybrid materials which have already generated a steady research interest because of their excellent properties such as high conductivity, high flexibility and light weight so as to be utilized in electronic component interconnections, electromagnetic interference shielding and electrostatic discharge protection.[3] Metalized plastic fabrics and fibres can enhance applicability of the metalized polymers because of their advantageous flexibility and wearability. They provide chances for photovoltaic applications on textile and clothing industry. Metallization is an attractive textile finishing process that adds value and improves functions of fashion products. One significant function of the metalized plastic textiles will be used as flexible and conducting electrodes of an innovative "wearable solar cell".

In this project, polyester fibre, a common type of synthetics fabric used in textile industry, is coated with metal to act as flexible electrode and also substrate for future photovoltaic application.

1.1.5 Prospective "wearable solar cell"

The innovative design of "wearable solar cell" has been developing faster in the past few years. Fibre-based solar cells have been successfully demonstrated and fabricated.[4-6] However, these phototypes still needs a lot of improvement before they can be used as "wearable solar cell". Hopefully one day in the coming future, the innovative solar cell will be popularly applied in daily life of human beings. People will dress fashionable clothing with photovoltaic devices and simultaneously convert solar energy to useful electricity energy for rechargeable electronic devices such as mobile phone.

1.2 Classification of flexible substrates

Currently, substrate materials for flexible applications can be classified into three major types, namely, metals, organic polymers (plastics) and flexible glasses. The properties of some typical examples of the major types are shown in Table 1.1.[7]

Property	Unit	Glass (1737)	Plastics (PEN, PI)	Stainless steel (430)
Thickness	μm	100	100	100
Weight	g/m^2	250	120	800
Safe bending radius	cm	40	4	4
Roll-to-roll processable?	–	Unlikely	Likely	Yes
Visually transparent?	–	Yes	Some	No
Maximun process temperature	℃	600	180, 300	1000
CTE	ppm/℃	4	16	10
Elastic modulus	GPa	70	5	200
Permeable to oxygen, water vapor		No	Yes	No
Coefficient of hydrolytic expansion	ppm/%RH	None	11, 11	None
Prebake required?	–	Maybe	Yes	No
Planarization required?	–	No	No	Yes
Buffer layer required? Why?	–	Maybe	Yes: adhesion, chemical passivation	Yes: electrical insulator, chemical passivation
Electrical conductivity	–	None	None	High
Thermal conductivity	W/m℃	1	0.1-0.2	16
Plastic encapsulation to place electronics in neutral plane	Substrate thickness	5x	1x	8x
Deform after device fabrication	–	No	Yes	No

Table 1.1 Properties of some Flexible Substrates

General speaking, anything thin is flexible. Rigid substrates like glass plate and stainless steel can be flexible if the thickness of the substrates is sufficiently thin.

For glass plate, it becomes flexible when its thickness is reduced to several $100\,\mu$ m. Glass can be thinned to $30\,\mu$ m as thin foil using downdraw method. It is light in weight but does not deform after device fabrication. Flexible glasses are the current standard substrates in flat panel display technology.

Metal substrates have high maximum process temperature of about $1000℃$, high electrical conductivity and opaque. In most cases, they are flexible if their thickness is less than $125\,\mu$ m. Flexible metals are attractive substrates to be used as emissive or reflective displays and applied on amorphous silicon solar cells for a long history.

Plastic substrates are highly flexible. Comparing with thin metal and flexible glass, polymers are easy to handle, inexpensive in material costs and light in weight. More importantly, plastics are a good option of substrates for flexible solar cells integrated into clothing due to its advantageous flexibility and permeable to oxygen and water vapour. However, the plastics are thermally and dimensionally instable as compared to the other two types of substrates. For most commercial polymers, barrier layers are coated in order to reduce absorption and permeability by gas, raise resistance to process chemicals, strengthen adhesion of device films, and reduce surface roughness.

In this project, the flexible substrates used are polyester which is a synthetic product often used in clothing industry. Among various polyester, polyethylene terephthalate (PET) is selected because it has high glass transition temperature (T_g) of

150℃ and good mechanical properties. The glass transition temperature of a plastic is very essential to be compatible with the device process temperature.

1.3   Fabrication of flexible electronics

Fabrication of electronic devices and systems including photovoltaics on flexible substrates have been growing rapidly and developing wide-openly within both the research and industrial community. Nowadays, there are TWO basic approaches that have been employed to make these flexible electronics.[7] The first one is the transfer-and-bond approach which transfers and then bonds completed circuits to a flexible substrate. The second approach is direct fabrication, i.e. the structure of the devices is directly fabricated on the flexible substrate.

In the first approach, the whole device structure is fabricated by their corresponding standard methods on a rigid-substrate like silicon wafer or glass plate. Then the structure is transferred to or fluidic self-assembled on a flexible substrate. This approach provides high-performance devices and has been applied on flexible wafer-based solar cell arrays. However, the production cost is high and the surface area coverage is small. It is possible to be applicable on large-area electronic surfaces at low density such as highspeed communication and lasing.

The second approach is the majority of fabrication for flexible electronics, both in

research and industry. It is simply expressed as the electronics being fabricated directly on flexible substrates. However, the direct fabrication needs to rely on polycrystalline or amorphous semiconductors because these materials can be grown on foreign substrates. Generally, the device performance is lowered due to low process temperatures tolerated by plastic substrates. It is significant to find out satisfactory balance between device performance and process temperature.

Among various process techniques based on the second approach, roll-to-roll manufacturing is the most promising technique and routinely used in industrial community to produce electronic devices on flexible substrates. It is high-throughput so that the fabrication cost can be reduced. A kilometer-long roll of thin plastic or metal foil is used as flexible substrate in the technology. New process techniques have been developed. The typical examples are printing of etch masks, additive printing of active device materials and the introduction of electronic functions by local chemical reaction.[7]

In this project, we will concentrate on the direct fabrication of the metal coating and ZnO layers on flexible plastic sheets and fibres by wet chemical reaction. This is the most direct way to manufacture large-area electronic surfaces, typically solar cells, and can be applicable in research laboratory and is also desirable for cost reduction. The substrates used were either two-dimensional (2D) planar sheet or

three-dimensional (3D) circular fibre which was both metalized as functional

electrodes using wet chemical technique.

1.4 Device structure of flexible solar cell

1.4.1 Basic structure of flexible solar cell

The simplest device structure of a flexible solar cell consists of flexible substrate,

bottom electrode, top electrode and active layer(s). The schematic diagram of a basic

structure of the flexible solar cell is shown in Figure 1.1. The essential requirement of

the electrodes is that either the bottom electrode together with the flexible substrate or

the top electrode must be optically transparent, in particular, transparent to solar

spectrum.
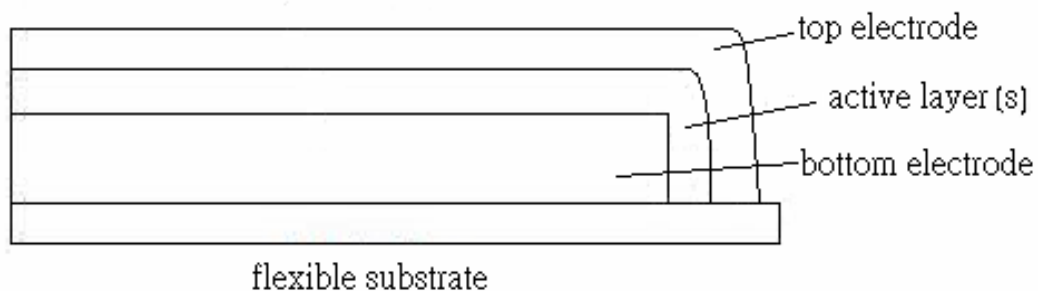
Figure 1.1　Schematic diagram of basic structure of flexible solar cell

The active layer should consist of both p-type and n-type materials. Three types of

active layer structure are proposed for future photovoltaic applications of our flexible

electrodes. They are (1) all polymers, (2) all inorganics, (3) hybrid inorganic-polymer type solar cells. For the proposed flexible solar cells, the substrate should be sufficiently flexible, light and low-cost, so plastic sheets or plastic fibres are chosen to be the substrate. Metal is chosen as the bottom electrode. Here the transparency is not the issue as the light will enter the active layer through the top electrode. The metal layer is produced by metallization. After that, active layers are fabricated to absorb light, generate photo-induced electron-hole pair and separate electron-hole pair to top and bottom electrodes to produce a photo-generated current in the photovoltaic device. Finally, top electrode is deposited above the active layers. It has to be transparent to allow incident light passing through and hence the active layers of certain band gaps can absorb light spectrum.

1.4.2   Flexible electrodes - metalized PET sheet and fibre

For any photovoltaic devices, conducting electrodes (both bottom and top electrodes) are necessary requirements. Except processing good conductivity, they need to have good mechanical properties such as flexibility for fabrication of flexible electronic. They should have good adhesion with the substrates. They are chemical stable and should be interact with the active layers and substrates. They also should be cheap.

In the project, we concentrated on the bottom electrodes. As mentioned in Sections 1.2 and 1.3, PET sheet and fibre were the flexible substrates. Metal layers such as nickel (Ni) or copper (Cu) were used as the bottom electrodes. Metal layers were chosen because they are inexpensive, possess good conductivity even they are very thin, have flat and smooth surface morphology. In this project, the metal layers deposited on the flexible substrates using wet chemical techniques.

1.4.3 Other parts of flexible solar cell

In this project, except the flexible bottom electrodes, vertical-aligned zinc oxide nanorod (ZnO nanorod) arrays used as the active layer on the metalized fibres were also explored. The ZnO nanorods were grown by a simple chemical bath deposition (CBD). The undoped ZnO arrays are intrinsic n-type.

The proposed active layers include three different types. The first one is the all-polymer type. The commonly used organic layer include two well-known organic materials, poly 3-hexylthiophene-2,5 (P3HT) and [6,6] phenyl C61 butyriacid methyl ester (PCBM). They are usually selected as the p-type and n-type organic semiconducting materials respectively. However, in this project, we did not use this type as they are very difficult to fabricate these two inorganic materials onto the fabrics. The second one is the all-inorganic type, i.e. both n-type and p-type materials

are inorganic materials which are usually oxides. The third one is the hybrid inorganic-polymer type, i.e. the n-type and p-type materials are inorganic and polymer respectively (It is easy to find a good n-type oxide and p-type polymer but not the vice versa). Hence for both the second and third types of structure, a n-type inorganic active layer will be needed. In this project, we concentrate on fabricating an n-type ZnO nanorod layer as the active layer. In the future, these ZnO/metal/PET fiber can be further developed into the second or third type solar cell by depositing a p-type layer (either polymer or inorganic) as well as a top electrode.

The necessary requirements of the top electrodes are sufficiently transparent, conductive and flexible. The electrode may be thin film aluminium (Al) whose thickness may be between fifteen and thirty nanometres. The other options of the top electrode are conducting polymer,[8-10] conducting oxide,[11,12] carbon nanotube,[13-15] graphene[16-18] and nanosilver.[19,20]

1.5   Metallization of Plastics

1.5.1   Introduction

Wet chemical technique for metallization has been a widely studied technology in industrial production since 1960s. The metallization is generally divided into two major types of plating. They are electroplating and electroless plating. Both types of

plating were applied in the project to coat required metal layers on the plastic sheet and fibre. The most important step of the metallization is the pretreatment,[21] including surface cleaning and surface etching using NaOH. After the pretreatment, activation and electroless plating were followed immediately. Thin metal layers of good conductivity were thus coated on the insulating surface of the plastic substrates. Furthermore, thicker metal layers are deposited on the initial conductive metallic films by electroplating process.

1.5.2 Surface cleaning

The quality of the metal coatings greatly depends on cleanliness and texture of the substrates. The surface should be free from oil and grease. In degreasing process, oil or grease were removed from surface of the plastic substrate by ultrasonic cleaning with detergents. Organic solvents such as ethanol and acetone should be avoided because the plastic substrate may be dissolved in these organic solvents.

1.5.3 Surface etching

After cleaning, the surface needed to be etched. No matter using physical or chemical etching, a rough surface was needed in order to make the deposition of metal layer easily. The texture of the plastic surface to be coated should be porous so

that catalytic substances could be attached to the plastic during the following process of activation. More significantly, the plastic surface is etched using chemical approach in order to obtain a functional surface with carbonyl and/or hydroxyl groups favored to subsequent electroless deposition.

Physical etching such as plasma treatments is limited by the size and shape of the plastic substrate which is not applicable to 3D circular fibre. Hence, chemical approach of surface etching was applied in this project. It was used to modify the chemical compositions of the substrate surface either by chemical reaction with a given solution (wet treatments) or by the covalent bonding of appropriate macromolecular chains to the substrate surface (grafting).[22] Since there is no restriction in the size and shape of the plastic substrate, wet treatments of surface etching were applied to modify the structure of the plastic substrate.

PET belongs to polyester containing ester functional group in the main chain. In general, plastics with the functional group facilitate the surface modification either by oxidation at the presence of concentrated chromic acid ($H_2Cr_2O_7$) or by hydrolysis at the presence of sodium hydroxide (NaOH).[22] Since traditional chromic acid etching is only suitable for plastic surface modification which consists of acrylonitrile butadiene styrene (ABS), hydrolysis was applied for surface modification of the PET substrates at the presence of sodium hydroxide. Hydrolysis of PET caused by sodium

hydroxide attacks was illuminated in Figure 1.2.
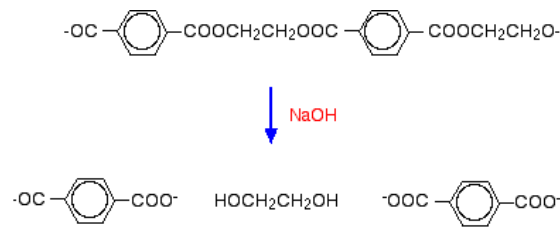
Figure 1.2   Hydrolysis of PET due to sodium hydroxide attacks

1.5.4   Process of metallization of plastics

Once the surface modification through etching is completed, there were three stages of metallization which are called sensitization and activation, electoless plating and electroplating to coat the required metal layers. The schematic diagram of plastic metallization is shown in Figure 1.3.[23]
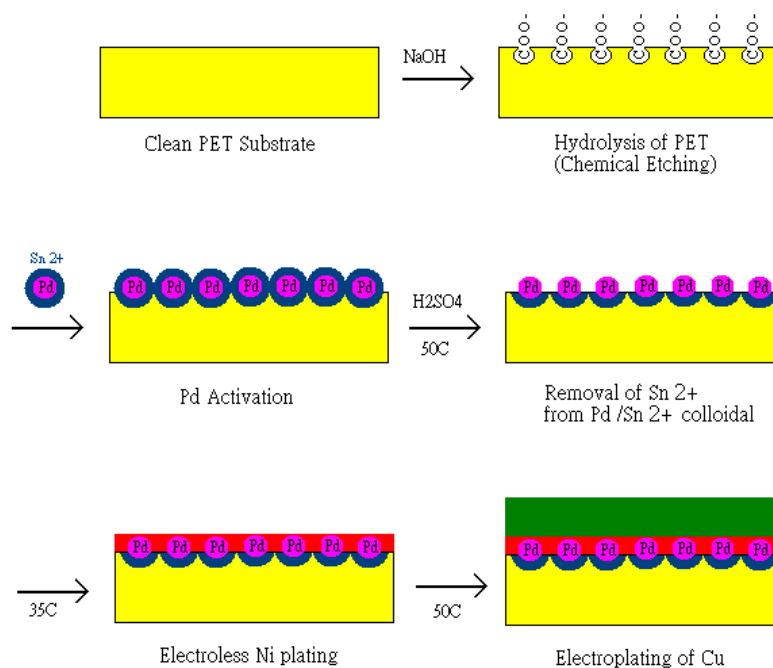
Figure 1.3   Schematic diagram of plastic metallization

1.5.4.1 Sensitization and Activation

Before depositing a metal layer on the plastic surface, the etched surface had to be sensitized and activated in order to achieve better adhesion between the plastic surface and the required metal coating. In this stage, Pd atom was used as catalyst because it has high metal ion adsorption ability. Therefore, metal ions are easily adsorbed on the Pd surface and reduced to metal layers.

The etched surface with active sites were introduced into acidic activation bath containing Palladium/Tin (II) (Pd/Sn^{2+}) colloidal. The surface was first sensitized by the absorption of Sn^{2+} ions in the Pd/Sn^{2+} colloidal. The cations formed complex bond with carboxylate salts which contained carboxylate (RCOO$^-$) ions at the active sites. Since Pd atom was surrounded by Sn^{2+} ions in the colloidal, it could be bonded to the plastic surface at the active sites. Sn^{2+} ions which exposes to the air were removed by diluted H_2SO_4 solution at a bath temperature of $50℃$. After that, the palladium was exposed at the plastic surface for further deposition of metal layers. Hence, the implanted Pd atom acts as a significant catalyst for the successive electroless Ni plating.

1.5.4.2   Electroless plating (auto-catalytic metal deposition)

Once the sensitization and activation of the etched surface had been carried out, an continuous, conductive and thin metallic layer was accumulated on the non-conductive plastic surface by electroless plating. Electroless plating, also known as auto-catalytic plating, is a non-galvanic method to coat metal layers by controlled chemical reduction that is catalyzed by the metal being deposited. There are several simultaneous reactions including oxidation and reduction which occur in an aqueous solution and without any electrical input from external power. The electron source is a soluble reducing agent R in the aqueous solution. In electroless plating process, R is oxidized near the plastic surface and hence electrons and corresponding product R^{n+} are generated.

$$R \longrightarrow ne^- + R^{n+} \tag{1.1}$$

Meanwhile, reduction of metal ion M^{n+} occurs to form metal M on the plastic surface where Pd catalyst has been implanted.

$$M^{n+} + ne^- \longrightarrow M \tag{1.2}$$

The overall process becomes

$$M^{n+} + R \xrightarrow{\text{Pd seed}} M + R^{n+} \tag{1.3}$$

The process is autocatalytic and a thin metal layer of uniform thickness is resulted because the driving potential is essentially constant at all points of the plastic surface.

In this project, electroless nickel plating which is a common electroless plating was used. The plastic surface, which had been processed with activation for adhesive bonding, was then coated with thin and conductive nickel layer before further plating. This electroless process gives useful adhesion force (about 10 to 60 N/cm), but is much weaker than actual metal-to-metal adhesion strength.[24]

1.5.4.3   Electroplating

Electroplating is the deposition of a metal coating on a conducting surface of a substrate with connection of an external electrical power supply. An ionic metal is supplied with electrons to form layer of a non-ionic coating on the substrate. A common system involves a power supply of direct current (DC), a chemical solution which contains a metal salt, two anode rods (positively charged) which can be soluble anodes or insoluble anodes and a cathode rod (negatively charged) where the substrate is placed. The soluble anode consists of the metal being plated, whereas the insoluble anode is usually carbon, platinum or steel. In the project, non-cyanide alkaline copper strike plating was applied on the electroless nickel layer at a temperature of $50℃$. The metal salt was a copper salt and stainless steel is the insoluble anode. The external electrical power was connected to the anodes and the cathode. At the cathode, electrons were supplied on the nickel layer. The metal salt contained positively

charged metal ions which were attracted to the negatively charged sample at the cathode and reduced to its metallic form. Hence, a thick layer of copper was deposited on the nickel layer of the plastic substrate in this manner.

1.6   Typical photovoltaic applications on flexible substrates

1.6.1   Introduction

In the project, the flexible electrodes and substrates for photovoltaic applications were the metal layers of Ni and/or Cu on the PET sheets and fibres. The metal-coated PET fibres were mainly designed and fabricated for the application of flexible solar cells integrated into clothing.

As mentioned in Section 1.1.3, the "third generation" is the turning point for the development of flexible solar cells which is low cost (mainly production cost), lightweight and capability to make different shapes which can be applicable in textile industry. As we mentioned before, there are several types of solar cells: (1) all-organic, (2) all inorganic and (3) hybrid inorganic-organic.

1.6.2   Organic solar cell

1.6.2.1   Organic photovoltaic materials

Organic electronic materials are conjugated solids where both optical absorption

and charge transport are dominated by partly delocalized π and π^* orbitals.

Candidates for photovoltaic applications are mainly small molecules and conjugated polymers. The small molecules are conjugated molecules with molecular weight of a few hundreds, which can be in form of crystalline or polycrystalline films, and even amorphous films. The films are prepared by vacuum deposition or solution processing. Different from the small molecules, the films of the conjugated polymers are commonly processed from solution.[25] One of typical examples of the conjugated polymers is poly(3-hexylthiophene) (P3HT). It has high optical absorption to solar spectrum and is thus a good option of electron acceptor in the cells.

1.6.2.2   Device concepts of organic solar cell

Device structures of organic solar cells can be divided into three major types.[12] The simplest one is homojunction structure which is a layer of organic material sandwiched between two different electrodes, typically a transparent conducting oxide such as indium tin oxide (ITO) and a metal contact of low work function such as Aluminum (Al). The difference in work function provides an electric field to drive photo-generated charge carriers towards the respective electrodes.

The second one is the heterojunction structure which is based on donor-acceptor system. The performance of this organic photovoltaic device has improved. At the

interface between two different materials, electrostatic forces are created due to the differences in electron affinity and work function. The interfacial electric field that drives charge separation in cases of both electron affinity and work function are greater in one material than the other. These strong local electric fields will break up the excitons (bound state of electron-hole pairs) if the differences in potential energy are larger than the exciton binding energy. The separated charge carriers reach to the corresponding contacts before recombination.

The last one is the structure dispersed heterojunction. The concept of donor-acceptor system is applied but the electron accepting and electron donating material are blended together to provide continuous paths exist in each material from the interface of the two materials to the electrodes. The separated charge carriers may be easier to travel to the contacts before recombination appears. Hence, photocurrent is generated and then delivered to the external circuit. Note that the domain size in either material of electron acceptor or material of electron donator needs to be similar with the exciton diffusion length, so that the exciton can diffuse to the interface and break up.

1.6.2.3   Typical example of organic solar cell

As proposed in Section 1.4.3, the organic solar cell of blended heterojunction

structure of P3HT as electron donor and PCBM as electron acceptor are suggested. It is one of most efficient structures of organic solar cell. P3HT has high optical absorption, whereas PCBM is one of the most soluble fullerene (large carbon-cage molecules) derivatives. For such kind of organic solar cell on rigid substrate of ITO glass, highest efficiency of 4.64% was obtained.[26]

This kind of photovoltaic devices can be applied on flexible polyester substrates, in particular, PET substrates. In general, the organic materials are commonly processed from solution and the annealing temperature of the device is 120℃, below glass transition temperature of PET (150℃).

1.6.3 Hybrid inorganic-organic solar cell

1.6.3.1 Contrast between hybrid inorganic-organic and organic solar cell

Hybrid inorganic-organic solar cells have been attracting extensive researches as charge transfer is favored between inorganic semiconductors of high electron affinity and organic materials of relatively low work function, compared with organic solar cells.

Photocurrent generation is affected not only due to bulk optical absorption, but also mechanism of exciton dissociation. Even though organic solar cells are low cost and possess to easy processing procedure and low fabrication temperature, however the

diffusion lengths of the excitons are short (typically 1-10 nm). For many conjugated polymers, electron mobilities are extremely low, typically below 10^{-4} $cm^2V^{-1}s^{-1}$, due to the presence of substantial electron traps such as oxygen.[27] Most excitons are broken up or recombined before reaching the contacts.

Hybrid inorganic-organic solar cell can take advantage of good charge transport. In term of power conversion efficiency, inorganic devices are over organic devices because intrinsic carrier mobilities of inorganic semiconductors are much higher. Higher carrier mobilities mean that charges are transported to the contacts more quickly so that current losses via recombination can be reduced.[27]

1.6.3.2　Hybrid nanorod-polymer solar cells

Since one-dimensional (1D) nanorods provide a direct path for transport of charge carriers, they are preferable to quantum dots in solar energy conversion. Hence, inefficient hopping electron transports are limited and resulting photovoltaic performance is improved. Moreover, the combination of semiconductor nanorods wrapped with the conjugated polymers such as P3HT can create transfer junctions with high interfacial area. The nanorod-polymer blend structure also provides superior flexibility, which has good match to the flexible substrate of the PET fibres. When the fibres bend to certain degrees of flexibility, the nanostructure may bear the bending

without crack formation, unlike thin film structure.

In this project, the semiconductor nanorods used are ZnO nanorods. ZnO belongs to II-VI semiconductor group and is intrinsically n-type material. Optically, it has a wide direct band gap of 3.37 eV and high electron mobility.[28] Vertical arrays of ZnO nanorod are grown on the metalized PET fibres using chemical bath deposition (CBD) technique.

1.7 Purpose of the research

In the project, the objective is to fabricate flexible and conducing bottom electrodes on flexible substrates including polyester sheets and fibres for typical photovoltaic applications.

The flexible solar cells, typically organic solar cell and hybrid nanorod-organic solar cell, mainly consider the application of "third generation" technology.

In the project, the work was divided into three stages which were closely related. The first stage was to fabricate metal coatings such as Ni and Cu on PET sheets. This was a starting point for the second stage which was to fabricate metal coatings on PET fibres. The third stage was to grow vertical-aligned arrays of ZnO nanorod on the Ni-coated PET fibres.

1.8 Contribution of the research

The major achievement of our work was to fabricate flexible and conducting bottom electrodes on polyester fibres.

Both the metalized PET sheets and fibres can be acted as the bottom electrodes of the organic solar cell as well as hybrid nanorod-organic hybrid solar cell, whereas the ZnO nanorod arrays of vertical alignment can be served as n-type material of the nanorod-organic hybrid solar cell on the polyester fibres.

This project provides flexible and highly-conducting electrodes in shape of 3-D circular fibre for wide range of applications including innovative "wearable solar cell" in textile industry.

1.9 Outline of the thesis

In this thesis, chapter 1 is a general introduction for the fabrication method (metallization) and applications of flexible electrodes of metal coatings on polyester substrates. The purpose and contribution of the research are notified as well.

Chapter 2 describes of characterization methods for the metal coatings on the polyester sheets and fibres. The characterization methods of vertical-aligned arrays of ZnO nanorod grown on the Ni-coated PET sheets as well as fibres are also explained.

Chapter 3 lists the fabrication and characterization results of the metal coatings of

Ni, Cu and Au on PET sheets, while Chapter 4 records the fabrication and characterization results of the metal coating of Ni and Cu on PET fibres. Chapter 5 mentions the fabrication and characterization results of the vertical-aligned arrays of zinc oxide nanorod on Ni-coated PET fibres.

Finally, chapter 6 is the conclusion of the project work and future development of the flexible electrodes.

CHAPTER 2　CHARACTERIZATION METHODS FOR FLEXIBLE ELECTRODES

2.1　Introduction

In this project, metal coatings including Ni, Cu and Au were deposited on both PET sheets and fibres which can be acted as flexible bottom electrodes for organic solar cell and hybrid nanorod-organic solar cell. Wet chemical technique for metallization had been applied to coat the metal layers on the flexible substrates. On the other hand, vertical-aligned ZnO nanorod arrays used as n-type material of the hybrid nanorod-organic hybrid solar cell had been grown on the metalized PET fibres via a chemical bath deposition (CBD).

Various characterizations of the bottom electrodes have been conducted. The transport properties of the metal layers coated on the PET sheets and fibres were investigated by a four-point probe. Current (I) - voltage (V) characteristics of the electrodes on PET sheets and fibres were performed so as to determine their resistivity as well as conductivity. Besides, structural properties of the flexible electrodes were studied. The surface and cross-sectional morphology of the metal coatings were observed by optical microscopy (OM) and scanning electron microscope (SEM). X-ray diffraction (XRD) was also used to characterize the phase

and crystallinity of the metal layers.

Similarly, both the structural and optical properties of the vertical-aligned ZnO nanorod arrays grown on the metalized polyester fibres were also characterized. XRD patterns and Raman spectra were used to identify the phases, crystallinity and orientation of the ZnO nanorods. Field emission-scanning electron microscope (FE-SEM) was employed to investigate the surface and cross-sectional morphology of the nanorods. Transmittance and photoluminescence profiles were measured to investigate the optical properties of the ZnO nanorods. The optical properties of the ZnO nanorods are important as they are potentially useful for photovoltaic applications.

2.2   Structural characterization

2.2.1   X-ray diffraction (XRD)

X-ray diffraction (XRD) is a common and non-destructive method to characterize crystal structure and determine atom location of different materials in form of bulk solids, powders or thin films.

Qualitative analysis of thin films based on XRD has been extensively used. By comparing the XRD patterns of an unknown material to a library of known patterns, the composition as well as phase of the unknown materials can be identified. In

general, each crystalline material produces a unique X-ray "fingerprint", XRD pattern with unique diffraction peaks, i.e. a graph of X-ray intensity versus scattering angle. The diffracted X-ray peaks from the crystalline materials must satisfy Bragg's Law:

$$2d \sin\theta = n\lambda, \quad n=1, 2, 3, \dots \tag{2.1}$$

where θ is the diffraction angle, d is the interplanar spacing and λ is the wavelength. The typical XRD system uses Cu K_α radiation (λ=1.54Å) and operates in Bragg-Brenyano (θ-2θ) geometry. The Cu K_β radiation is normally filtered by a Ni filter, leaving Cu K_α radiation as the X-ray source.

In the project, X-ray diffraction (XRD) was performed in a D8 Advanced diffractometer (Bruker) using θ-2θ configuration. The qualitative analysis of both the metal coatings and the ZnO nanorods grown on top of the metal coatings were undertaken. Planar sample surfaces usually have better XRD patterns. Thin metal layers on top of the PET fibres which are around 125μm in diameter were difficult to be examined. Therefore, only the thin layers deposited on top of the PET sheets under same experimental conditions as that on the fibres were characterized. ZnO nanorods grown on PET sheets had also been examined.

2.2.2   Scanning electron microscope (SEM)

Scanning electron microscope is a powerful tool for surface and cross-section

morphology analysis to give complementary information about the nature of samples studied. It images the samples by scanning them with high-energy electron beams (e-beams) in a high vacuum system, detecting signals back from the samples and displaying in raster scan patterns.

The limit of spatial resolution of the SEM which largely depends on the size of the electron spot is seriously considered for materials characterization. The resolution of conventional SEM is about few hundreds nanometer which is insufficient for structural characterization of ZnO nanorods of size less than hundred nanometer. Therefore, in this project, JSM-6335F (JEOL) field-emission scanning electron microscope (FE-SEM) was used rather than conventional SEM to study the ZnO nanorods. FE-SEM has a field-emission cathode in the electron gun to provide narrower e-beams of high energy, resulting in an improved spatial resolution to around ten nanometers. The charging and damage of the samples can also be minimized.

Optical microscopy (OM) (Nikon Microphot-FXA) has been used as a supplementary technique for SEM. It is noticed that insulating or poorly conducting samples needs a conductive coating such as gold (Au) to prevent charging of the samples before putting into SEM's chamber and thus obtain clear images of high resolution.

2.2.3   Raman spectroscopy

Raman spectroscopy is a light scattering technique and uses lasers as an excitation source. It can be used for micro-structural analysis and characterization of specimens with better sensitivity compared to XRD. The specimens can be of a very small volume that is below 1 μ m in diameter and don't need to be fixed or sectioned.

When incident laser interacts with a specimen having molecular vibration, no matter inorganic or organic material, vibrational information which is specific to the chemical bonds and symmetry of the specimen are obtained. Hence, Raman peaks with different Raman shifts provide a fingerprint such that the specimen can be identified.[29]

Raman shift is characteristic of the excitations that occur in the specimens, since it is a frequency shift due to the difference in photon energy of final state and initial state. It is expressed in wavenumbers, commonly in unit of inverse centimeters (cm^{-1}), and represented by

$$\Delta\omega = \left(\frac{1}{\lambda_0} - \frac{1}{\lambda_1} \right) \tag{2.2}$$

where $\Delta\omega$ is Raman shift, λ_0 and λ_1 are the excitation and Raman spectrum wavelength.

In the project, specimens of polyester sheets and fibres as well as the ZnO nanorods were identified using HR-800 Raman spectroscopy (Jobin Yvon). Compared with XRD, Raman spectroscopy can directly identity these ZnO nanorods grown on top of Ni-coated circular PET fibres, as well as planar sheets. The laser excitation wavelength of the Raman microscopy used for the specimens is 488 nm (blue colour).

2.3 Electrical characterization

2.3.1 Resistivity measurement

The transport properties of the metal layers including Ni and Cu coated on the PET sheets and fibres were investigated through I-V curves. Hence, by measuring the dimension of the coatings on PET sheet as well as fibres, quantitative values of resistivity and even conductivity of the metal layers can be found out.

The most common method for measuring resistivity is the four-point probe method.[17] The key advantage of the method is that the separation of current and voltage probes eliminates the impedance contribution due to wiring and contact resistances. It has a correction factor which depends on the deposition alignment of the four probes and the shape and size of the samples as shown in Figure 2.1. The probes are equally spaced with spacing *s*. A small current from a constant-current source is passed through the outer two probes and the voltage is measured between

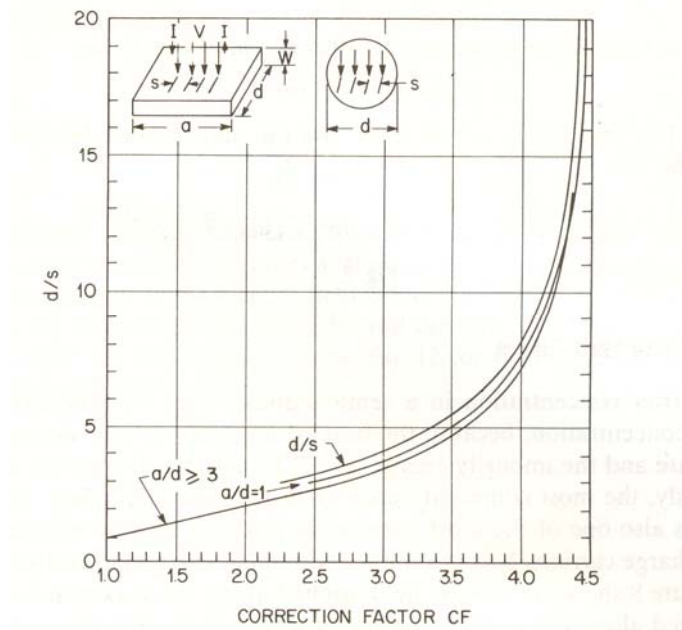the inner two probes as shown in the inset of Figure 2.1.[30]

Figure 2.1   Correction factor for resistivity measurement using four-point probe

based on the dimension of the samples

For a thin semiconductor plate with thickness W which is much smaller than either

length a or width d (in case of circular disc, diameter d) the resistivity is given by

$$\rho = \frac{V}{I}.W.CF$$

(2.3)

where CF is the correction factor shown in Figure 2.1.

Conductivity is the inverse of resistivity, which is simply represented by

$$\sigma = \frac{1}{\rho}$$

(2.4)

Both resistivity and conductivity are important material parameter and indicate how

good the electronic transport properties of charge carriers in the coated metal layers.

They depend on type and texture of different materials.

2.4   Optical characterization

2.4.1   Transmittance measurement

Optical transmittance measurement can determine bandgap energy of a semiconductor material.[31] Consider an epitaxial layer of material with thickness d deposited on a transparent substrate, the semiconductor's absorption coefficient, α (E), is given by

$$\alpha(E) \propto \sqrt{E - E_g} \tag{2.5}$$

where E is photon energy and E_g is bandgap energy.

When a beam of light (photons) is incident on the semiconductor, the intensity I is expressed as

$$I = I_0 \exp(-\alpha d) \tag{2.6}$$

where I_0 is intensity of the light incident on the semiconductor.

The light incident will be partially reflected due to Fresnel reflection at the air-semiconductor, semiconductor-substrate and substrate-air interfaces denoted by R_1, R_2 and R_3 respectively. At the lower end of the semiconductor layer, light intensity I_s becomes

$$I_s = I_0 \, (1 - R_1) \exp\left(-\alpha \, d\right) \tag{2.7}$$

If the substrate has surface roughness, there will be optical scattering losses at the substrate surface. Assuming that the fraction of light that does not reach the detector due to the scattering losses is S and both interference effects and multiple reflections are neglected, then light intensity via the layer and the substrate, $I_{transmitted}$, becomes

$$I_{transmitted} = I_0 \, (1 - R_1) \, (1 - R_2) \, (1 - R_3) \, (1 - S) \exp\left(-\alpha \, d\right) \tag{2.8}$$

Hence, the optical transmittance measured at the detector, $T(E)$, is given by

$$T(E) = \frac{I_{transmitted}}{I_0} = (1 - R_1) \, (1 - R_2) \, (1 - R_3) \, (1 - S) \exp\left(-\alpha \, d\right) \tag{2.9}$$

The absorption coefficient $\alpha(E)$ is thus solved from equation (2.9) to yield

$$\alpha(E) = -\frac{1}{d} \ln\left(\frac{T(E)}{(1 - R_1)(1 - R_2)(1 - R_3)(1 - S)} \right) \tag{2.10}$$

Neglecting Fresnel reflections and scattering losses, the transmittance data are normalized such that $T_{normalized} = 100\%$ in the transparent region ($E < E$g i.e. $\alpha = 0$). Equation (2.10) can be rewrited as

$$\alpha(E) = -\frac{1}{d} \ln\left(T_{normalized}(E) \right) \tag{2.11}$$

According to equation (2.5), $\alpha(E)$ has a square-root dependence on E where $\alpha(E)$ is determined by equation (2.11). Accordingly, $\alpha(E)^2$ has a linear dependence on E. Therefore, the value of bandgap energy is obtained by plotting $\alpha(E)^2$ versus E and extrapolating the linear part of the measurement to zero.

In fact, ZnO is a II-VI semiconductor material. The bandgap value of the ZnO nanorods grown on transparent PET sheets without any metal coatings can be determined using this transmittance method. The experiments were done in the wavelength ranges of ultra-violet to visible spectrum by a UV-VISIBLE spectrophotometer (UV-2550) at room temperature.

2.4.2 Photoluminescence measurement

Photoluminescence (PL) is an important technique for measuring the purity and crystalline quality of semiconductors. It is a process in which a substance absorbs and then re-radiates photons, in other words, electromagnetic (EM) radiation. Their photoluminescence spectra are measured to characterize the optical as well as crystalline quality of the semiconductors.

In this project, the room-temperature photoluminescence characteristics of the ZnO nanorods were studied under out-of-plane optical excitation caused by a Continuum 9100 Q-switched Nd:YAG laser (266 nm) at pulsed operated at 10 Hz with linewidth of 6 ns. The scattering signal was then collected by a lens and directed to an entrance slit of a monochromator which had a photomultiplier tube connected to its exit slit.

CHAPTER 3   FABRICATION AND CHARACTERIZATION OF METAL COATINGS ON POLYESTER SHEETS

3.1   Introduction

3.1.1   Objective

As remarked on Section 1.7, there are three main stages for the fabrication of flexible electrodes for photovoltaic applications.

In the first stage, the aim was to fabricate flexible electrodes of good conductivity, flexibility, uniformity and proper work function on 2D planar PET sheets. The flexible electrodes, acted as bottom electrodes for flexible solar cells, were metal coatings of gold (Au), nickel (Ni) or copper (Cu) deposited on PET sheets. The success of the first stage was a necessary starting point for the second stage. In the second stage, metal coatings were fabricated on 3D circular polyester fibres. In both the first and the second stages, wet chemical techniques for metallization were applied to coat the metal layers on the polyester sheets as well as fibres.

The simplest flexible solar cell for which our flexible electrode can be applied will be the organic solar cell. The schematic diagram of the organic solar cell is shown in Figure 3.1.
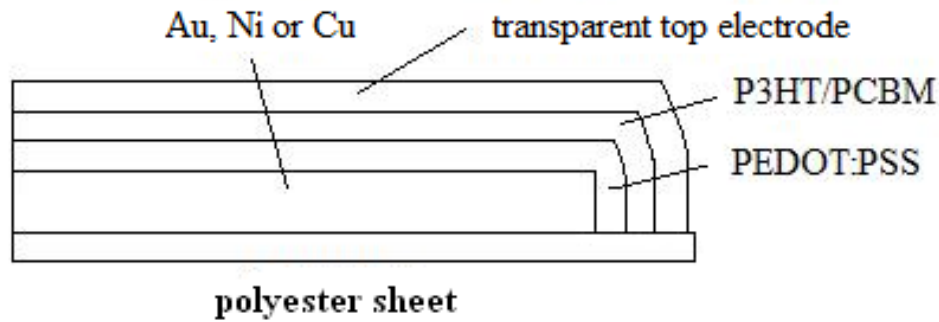
Figure 3.1   Schematic structure diagram of the organic solar cell

In this geometry, the flexible substrate is the PET sheet. Metal layer of Au, Ni or Cu is coated on the polyester sheet by wet chemical method. Two layers of organic films, PEDOT:PSS layer and the blend P3HT/PCBM layer (photoactive layer), are then deposited on top of the metal layer. PEDOT:PSS, which has high hole mobility, serves as electron blocking layer. For photoactive layer, P3HT is a polymer using as an electron donor which has high light absorption, whereas PCBM is an electron accepting fullerenes. They are blended together to yield a dispersed heterojunction. Lastly, transparent top electrodes of thin Al film or modified PEDOT:PSS layer are patterned on top of the photoactive layer.

3.1.2   Flexible electrodes of appropriate work function for organic solar cells

The organic solar cell as shown in Figure 3.1 is dispersed heterojunction which is based on donor-acceptor system and its photoactive layer is a blend layer of organic materials. In this configuration, conducting electrode of higher work function is usually connected to the positive terminal (anode) and electrode of lower work function is connected to the negative terminal (cathode). The bottom electrode used is Au with work function of 5.1 eV and the transparent top electrode is a thin layer of Al with work function of 4.28 eV. The energy-band diagram of this donor-acceptor system of the organic solar cell is illustrated in Figure 3.2.[25, 32, 33]
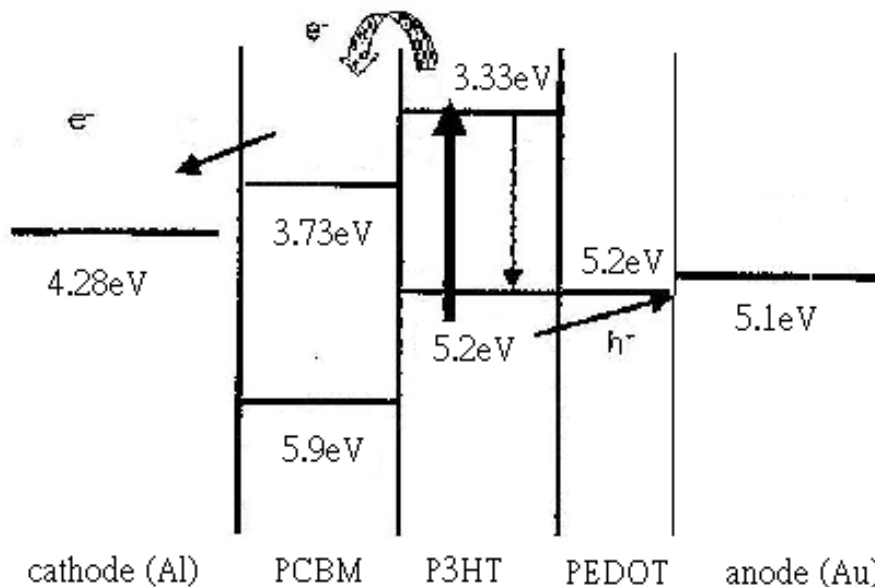
Figure 3.2   Schematic energy-band diagram of the organic solar cell

If both the excited state (LUMO) and ground state (HOMO) of P3HT (the donor

material) lie at energies sufficiently higher than those of PCBM (the acceptor material), then it is energetically favorable for an exciton reaching the interface to dissociate, leaving a positive charge carrier on the acceptor and a negative charge carrier on the donor. For efficient photocurrent generation, charge separation should complete successfully with electron-hole pair (EHP) recombination after a photon absorption event, and transfer to contacts should complete with interfacial recombination.

Moreover, if the domain size in the blend is similar to the exciton diffusion length, then the probability that an exciton will reach the interface and dissociation is high. For efficient photocurrent collection, each material must provide a continuous path for the transport of separated charge to the contacts. Isolated domains can trap charges, causing recombination.[25]

Al is widely used as the cathode of organic solar cells with a work function of 4.28 eV. The work function of Ni and Au are 5.15 eV and 5.1 eV respectively, while the work function of Cu is 4.65 eV.[33] In this case, Au and Ni have higher work function than Cu and they are more appropriate to be used as anode so that efficient photocurrent generation as well as good power conversion efficiency will be achieved. Therefore, Ni- or Au-coated PET substrates are more preferable as the flexible electrodes instead of Cu-coated substrate in the application of organic solar cell.

However, in this project, we do not focus on fabricating these organic solar cell devices. Firstly, several groups have been fabricated this geometry with ITO coated PET.[34-36] Secondly, in this project, we focused on using zinc oxide as the active layers. The main factor using the inorganic material over the organic materials is high intrinsic carrier mobilities that exist in inorganic semiconductors. Higher carrier mobilities mean that charges are transported to the electrodes more quickly so that current losses via recombination can be reduced and superior efficiency can be obtained.[27]

3.2   Methodology

3.2.1   Fabrication methods - metallization

In this chapter, various metallization processing parameters were investigated in order to achieve certain metal layers of good conductivity, flexibility, adhesion and uniformity. The established process of metallization consisted of four major stages: pretreatment, activation, electroless plating (autocatalytic metal deposition) and building-up deposition.[23] The pretreatment included surface cleaning and etching (surface modification). The activation and electroless plating followed the pretreatment immediately so as to produce a thin metal layer of good conductivity on the insulating surface of the polyester substrates. Building-up deposition of thicker

metal layer is further deposited on the initial conductive metallic films.

To deposit the thin Ni layer onto the PET sheet, the PET sheet was first etched with a 4M NaOH solution for 10 min. After the formation of a rough surface by etching in NaOH, the PET sheet was put into a MACuPlex activator D-34C concentrate bath, consisting of deionized water, 32% HCl, sensitizer 78 and MACuPlex activator D-34C concentrate for 3 min. This activation process allowed Pd particles to be filled into the voids at the sample surface which were formed by the etching process. The activated samples were then dipped into 50 g/L H_2SO_4 at 50℃ for 1 min, and then followed by electroless Ni plating at 35℃ for 6.5 min. The electroless Ni plating bath comprised deionized water, NH4OH, MACuPlex J-60 and MACuPlex J-61.

To deposit the thick Cu layer onto the Ni-coated PET sheet, the sample surface was first cleaned using electrolytic degreasing. After the surface cleanness, the sample was dipped into dilute H_2SO_4 at 20℃ for 15 s and then put into non-cyanide alkaline Cu strike plating bath including Cu salts and brightener. Current density of 2.5 A/dm^2 was applied at 50℃ for 5 min.

3.2.2 Use of NaOH for surface etching of PET

As mentioned in Section 1.5.3, the solution used for surface etching of the PET sheet and fibre was sodium hydroxide (NaOH).

PET belongs to polyester which contains ester functional group $[-\overset{O}{\underset{}{C}}-\overset{-}{O}-]$ in the main chain. This ester functional group, composing of an alcohol group (-OR') and an acyl group (RCO-) or equivalently, can be divided into carboxylate (RCOO-) and alkyl (-R') groups where R and R' represent alkyl groups which may be the same or different. The structures of ester group and PET are shown in Figure 3.3.
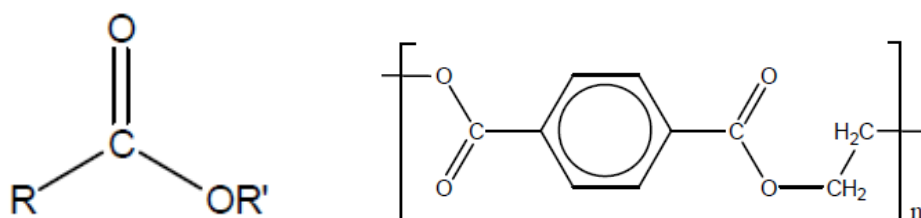
Figure 3.3   Structures of ester group (left) and PET (right)

PET facilitates the surface modification by hydrolysis at the presence of sodium hydroxide as shown in Figures 3.4 and 3.5.[23] There are electron-deficient carbon atoms on the PET surface. Nucleophilic species which contains a free pair of electrons can easily attack the carbon atom on the PET surface in order to donate an electron-pair to the electrophile (electron-lover) to form a chemical bond in reaction solution. Sodium hydroxide is a good nucleophilic agent to implement hydrolysis of PET and yield carboxylate salt (carboxylate group) and alcohol. The carboxylate salt which contains carboxylate ions (RCOO⁻ ions) is feasible to form metal complex with

Pd/Sn^{2+} colloidal at the active sites on the PET surface in Pd-activation bath. The

hydrolysis process significantly increases the number of carboxylate groups, which

then facilitates subsequent electroless Ni-plating.
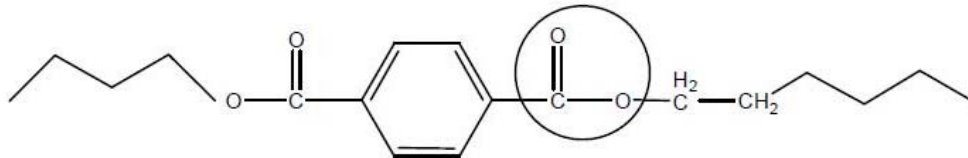
Fig. 3.4   PET surface modified by hydrolysis. Circles indicate the site of reaction
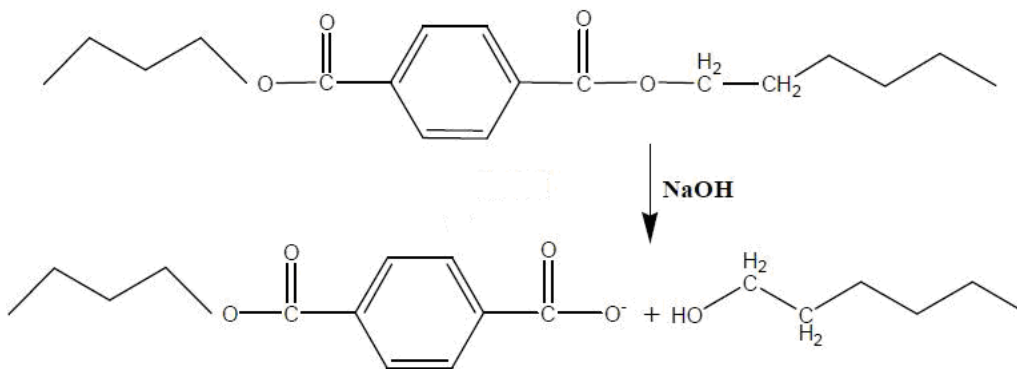
Fig. 3.5   NaOH attacks on PET

After etching, holes/voids with active $[-\overset{O}{\underset{\parallel}{C}}-\overset{-}{O}-]$ bonds existed. These holes/voids

will assist the Pd/Sn^{2+} ions to be deposited onto these sites with good adhesion.

The difference in key steps of the metallization of the Ni-, Cu- and Au-coated

polyester sheets are simply displayed as follows:

For Ni-coated PET sheet,

$$\text{electroless Pd-activation} \Rightarrow \text{electroless Ni-plating}$$

For Cu-coated PET sheet,

$$\text{electroless Pd-activation} \Rightarrow \text{electroless Ni-plating} \Rightarrow \text{electro-deposition of Cu}$$

For Au-coated PET sheet,

$$\text{electroless Pd-activation} \Rightarrow \text{electroless Ni-plating} \Rightarrow \text{electro-deposition of Au}$$

Obviously, the three types of metal coating had the two common major steps of electroless Pd-activation and Ni-plating. Usually, around 250 nm thick Ni layer was coated on the PET sheet. For the Cu-coated substrates, there was one more step of Cu electro-deposition, whereas for the Au-coated substrates, the additional building up deposition was electro-deposition of Au. However, for Au-coated and Cu-coated PET sheets, the thickness of the electroless Ni-plating layer was usually smaller than that of the Ni-coated PET sheet layer.

3.2.3 Characterization methods

Electrical properties of the metal layers coated on the PET sheets were examined using four-point probe so as to determine their sheet resistance and hence the conductivity on the planar substrate. Four-point probe method instead of the two-point probe method was used in order to eliminate contribution arise from wiring and contact resistances. Furthermore, the structural properties of the metal layers were investigated using X-ray diffraction (XRD). Surface morphology of the metal coatings was simply studied using optical microscopy (OM)

3.3 Results and discussion

3.3.1 Conductivity of the metal-coated PET sheets (four-point probe)

Electrical property of the metal layers coated on the PET sheets of sample size 2x2 cm^2 was examined using four-point probe to determine the resistivity as well as conductivity of the electrodes. The probes were spaced with equal spacing of 0.2 cm. Small current from a constant-current source was passed through the outer two probes and the voltage was measured between the inner two probes. I-V graphs of the Cu, Au and Ni layers coated on the planar sheet (Figure 3.6) indicated that all the metal coatings were ohmic. This showed that the three coated layers were good conductors.
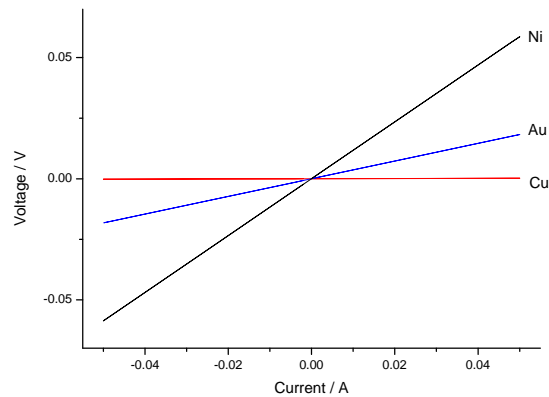
Figure 3.6   I-V graphs of Cu-, Au- and Ni-coated PET planar sheets

Based on the thickness obtained before, the calculated values of resistivity and conductivity of the three metal coatings are displayed in Table 3.1. These values indicate how good the carrier transport properties of the coated metal layers. It is noticed that Cu has a better conductivity as compared to the two other metals.

Metal layer	R(Ω)	Thickness (μm)	ρ (Ω/m)	σ (S/m)
Cu	0.0039	2.381	3.92E-08	2.55E+07
Au	0.3652	0.454	7.00E-07	1.43E+06
Ni	1.1746	0.238	1.18E-06	8.47E+05

Table 3.1   Resistivity and conductivity of the metal layers on PET sheet

The Cu layer obviously had the best conductivity among the three types of metal coating; while the Au layer had a better conductivity than that of the Ni layer.

According to standard values of the resistivity of the types of three metals at 20℃ as shown in Table 3.2,[37,38] all three metal layers formed on the PET sheet using metallization method had larger resistivity than the standard ones.

Material	ρ (Ω/m) at 20℃
Cu	1.68E-08
Au	2.44 E-08
Ni	6.99 E-08

Table 3.2   Resistivity of Cu, Au and Ni at 20℃

Even though the resistivity of the Cu layer had the same order of magnitude, it was about two times larger than the standard one. On the other hand, the resistivities of the Au and Ni layers had one order of magnitude larger than the corresponding standard values. The possible reason for the metal layers grown on PET sheets to have larger resistivity was the existence of defects such as pitting sites and surface cracks. Non-uniform thickness of the metal layers probably caused larger resistivity than the standard ones as well. As the thickness of Cu layer was the largest among the three metal coatings, both pitting sites and surface cracks would be less in Cu layer as observed in Figure 3.8. Thus, better conductivity was expected in Cu layers. Au was also deposited using electro-deposition.

3.3.2 XRD and surface morphology of metal-coated PET sheets

The structural property of the metal coatings on the PET sheet was investigated using XRD method. The XRD pattern with 2-theta range between 20° and 80° of the metal coating of Cu grown on pure PET substrate was shown in Figure 3.7.[23, Appendix A] Besides, surface morphology of the metal-coated PET sheets was studied using optical microscopy (OM). The surface images of the metal coatings on PET sheets were displayed in Figure 3.8.
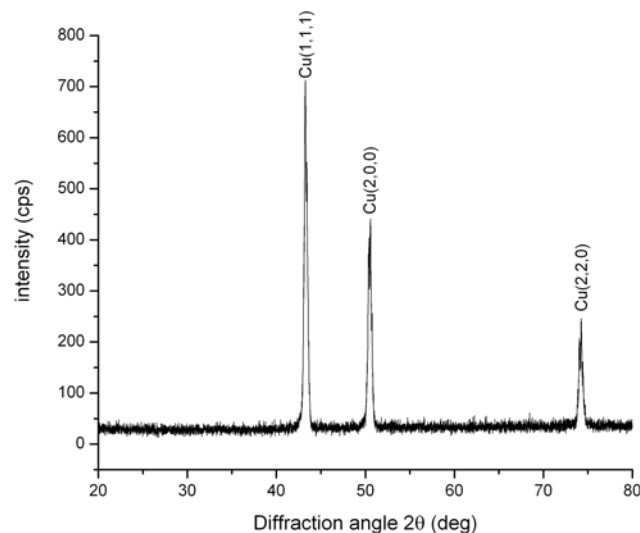
Figure 3.7   XRD pattern of Cu-coated PET substrate

Diffraction peaks located at diffraction angles of 2-theta =43.3°, 50.4° and 74.1° which referred to lattice plane (111), (200) and (220) were observed. Only sharp Cu(111), Cu(200) and Cu(220) peaks were observed indicating that the obtained Cu

was of single phase with good crystallinity and no preferred orientation. Hence, good

quality of Cu coating on PET substrate was formed via electro-deposition method.
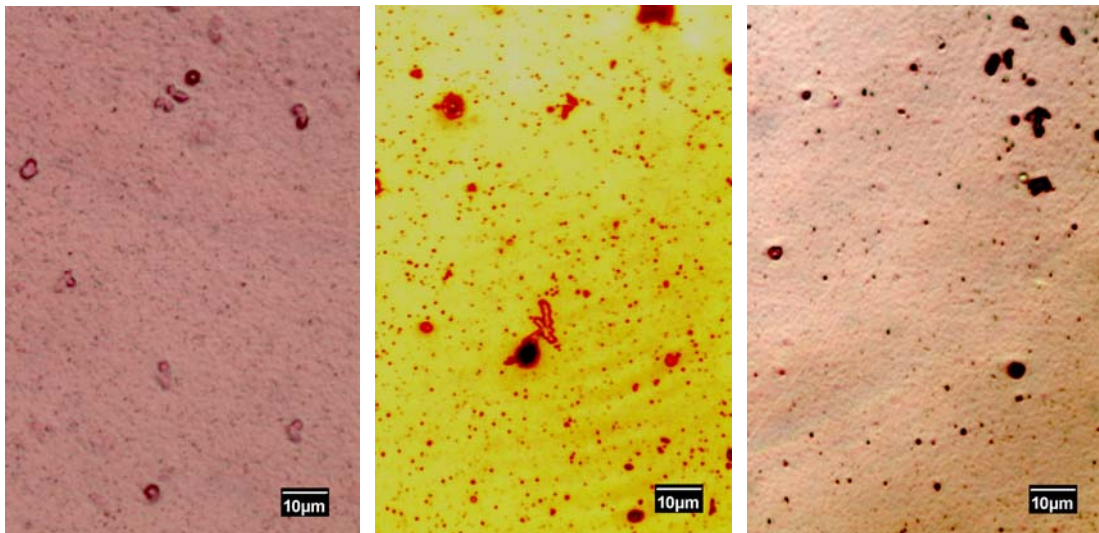
Figure 3.8   Surface images of Cu (left), Au (middle) and Ni (right) coated on PET

sheets

Figure 3.8 shows the surface morphology of these different metal coatings. General

speaking, pitting sites of diameter ranging from one to several microns were observed

on the surface. However, among the three metal coatings, the Cu layer had the least

amount of surface defects due to a larger thickness.

3.4   Conclusion

Metal coatings of Au, Ni and Cu on 2D planar PET sheets acting as the bottom electrodes of the flexible solar cells were successfully fabricated via a wet chemical techniques for metallization. It was an important starting point to fabricate flexible bottom electrodes on 3-D circular PET fibres using the same technique.

The electrodes obtained were highly conductive and flexible. In the application of organic solar cells, the Ni or Au coating has a more appropriate work function for the application of organic solar cells, as compared with Cu coating.

The four-point probe measurement verified that the fabricated metal coatings were ohmic conductors. The ascending order of conductivity for the flexible electrodes was found to be Ni, Au and Cu. As expected, the obtained resistivities of the metal coatings were larger than the corresponding bulk values for the same material. It was probably due to the formation of defects such as pitting sites (diameter ranged from one to several microns) and non-uniform thickness of the metal layers.

The observation of XRD peaks of Cu(111), Cu(200) and Cu(220) indicated that the metal coating of Cu on PET substrate was of single phase with random orientation. The wet chemical for metallization resulted in high-quality metal layers on the PET substrate.

CHAPTER 4   FABRICATION AND CHARACTERIZATION OF METAL COATINGS ON POLYESTER FIBRES

4.1   Introduction

4.1.1   Objective

In the second stage of the project, the objective was to fabricate conductive, adhesive and flexible electrodes on circular PET fibres. The flexible electrodes used were metal coatings of nickel (Ni) and copper (Cu). Similar with the fabrication of flexible electrodes on polyester sheets, wet chemical techniques for metallization were applied to coat the metal layers on polyester fibres.

The polyester fibres have three dimensional (3D) geometry and small circular size of around 125 μ m in diameter, whereas the polyester sheets are two dimensional (2D) of planar surface on which the metal coatings can be easily deposited. Hence, the deposition of the metal layers on these circular PET fibres was much more difficult than that on the PET sheets. The fabrication of conductive, adhesive and flexible electrodes on the metal-coated polyester fibres was a hard challenge.

4.1.2   Structure of the bottom electrode on PET fibres

The schematic diagram in Figure 4.1 shows the geometry of the bottom electrode formed on a flexible PET fibre.
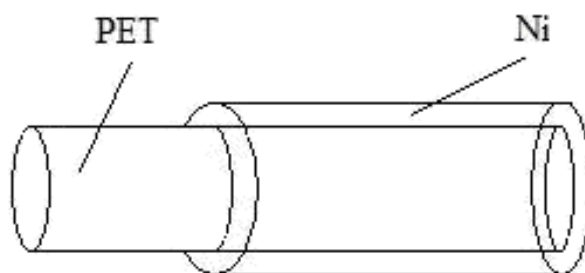
Figure 4.1   Schematic diagram of bottom electrode formed on PET fibre

As shown in the diagram, major part of the PET fibre (T1203-1 #37) was coated with a Ni layer and leaving one end of the fibre to be uncoated. As shown in Section 3.1.2, Ni layer has high work function which is an appropriate anode option for organic solar cells.

4.2   Methodology

4.2.1   Fabrication problems for metal coatings on 3D circular fibre

In case of 2D planar PET sheet, a thin Ni layer was formed immediately after dipping the etched and activated substrate into the electroless Ni bath. However, unlike planar PET sheet, no metal coating was formed on the surface of the circular fibres when the etched and activated 3D circular fibres were dipped into the

electroless Ni bath for one hour. Indeed, no matter how long the treatment time of the fibres in the electroless Pd-activation as well as Ni-plating baths used, there was still no metal layer to be observed. Similarly, changing the NaOH etching times during the surface modification process did not show any improvement. No metal layer could be successfully formed on the surface of the circular fibres. In order to coat Ni layer on the PET circular fibres, two techniques had been developed.

4.2.2 Techniques to improve the metallization of 3D circular fibre

Two modified techniques for metallization had been used so as to deposit metal layer successfully on the PET fibres. Schematic diagrams of the two modifications for metallizing PET fibres were shown in Figures 4.2 and 4.3.

The first modification was that the fibres were placed at the side of the beaker instead of submersing inside the solution at the bottom of the beaker during the metallization process as shown in Figure 4.2.
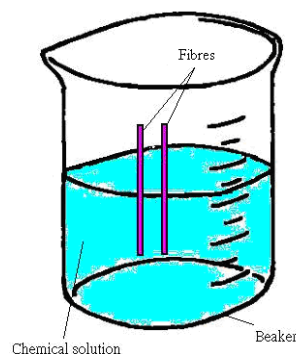
Figure 4.2   First technique modification of metallization

By placing the fibres on the side of the beaker, metal layer was found to be coated on the surface of the fibres. However, even though the metal layer was formed on the PET fibre surface, only discontinuous and non-uniform metal-coated layer was formed on the surfaces of the fibres. Indeed, the metal coating formed usually on the surfaces of fibres which were in contact with the beaker's edge. Furthermore, the formation of the metal coating using this modification was not repeatable, i.e. the metal-coated PET fibres were not fabricated successfully for every trial. In order to improve the coating quality, second modified technique was applied to replace the first method for metallization of the PET fibres.

In the second technique, the two ends of the PET fibres were first thermally bonded onto the PET sheet as shown in Figure 4.3. The whole sample, including fibres and plastic sheet, was then dipped into the corresponding chemical baths for metallization.
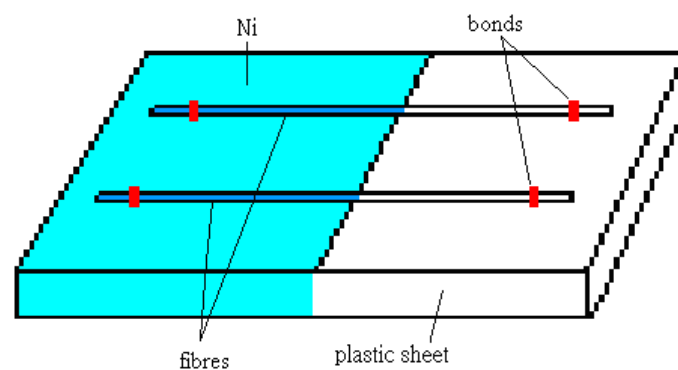
Figure 4.3   Second technique modification of metallization

With the assist of the plastic sheet, continuous metal-coated layer was successfully deposited on the fibres. Furthermore, this modified process had been demonstrated to be a repeatable process. However, the detailed mechanism of the second modified technique of metallization was still unknown.

4.2.3 Metallization parameters and characterization methods

Surface etching of the PET fibres were performed using various processing parameters including concentration of NaOH solution, etching time and temperature of the NaOH bath, deposition time of Pd-activation and Ni-plating baths. The effects of these five processing parameters on the qualities of the Ni coatings were investigated.

The structural properties of these coated fibres under various processing conditions were studied. The surface and cross-sectional morphology of the metal coatings were observed by optical microscopy (OM) and scanning electron microscope (SEM) respectively. Besides, the transport properties of the metal layers were investigated by studying their I-V characteristics.

4.3 Results and discussion

4.3.1 Surface morphology of the Ni-coated PET fibres due to surface defects

Optical micrographs showing the surface defects formed on Ni-coated PET fibres were obtained by optical microscope. Figure 4.4 shows the two images obtained by the optical microscope. The fibres were etched with 4M NaOH solution at 20℃ for ten minutes and then the treated samples were immediately dipped in a Pd-activation bath and successive Ni-plating bath both for three minutes. On the surface of the PET fibre, small cracks were clearly observed. The formation of the cracks was probably due to the difference in thermal expansion coefficients of Ni metal and PET substrate. In fact, the coefficients of linear expansion, at 20℃, of Ni metal and PET polymer are 13.3×10^{-6}/℃ and 117×10^{-6}/℃ respectively.[39] The big difference in linear thermal expansion coefficients at room temperature makes cracks form easily because of the heating process during electroless Ni-plating operated at 35℃. In this case, small cracks of the Ni layer were easily formed on the PET fibre. Obviously, electrical performance of the metal coating would be lowered down due to the existence of these small cracks.

Another type of defect was the pitting sites formed on the surface of the Ni-coated PET fibres. In the Pd-activation bath, polyethylene glycol (PEG) was existed in the bath in order to couple with hydrophobic (water-fearing) molecules to produce

non-ionic surfactant which lowers the surface tension of these hydrophobic molecules. However, PEG might oxidize the Sn^{2+} ions and form Sn^{4+} ions in the Sn^{2+}/Pd colloidal. Once the oxidation had occurred, the oxidized Sn^{4+}/Pd colloidal preferably accumulated together and hence black precipitates were formed.[23] These black precipitates would probably generate pitting sites on the surfaces of the fibres. It is reasonably to believe that the pitting sites increase the surface roughness of the metal coating. The size of the pitting sites was found to be around 1μm in diameter. This value is too large for the fibres being applied as the substrates and bottom electrodes of thin film devices. Normally, thickness of thin film devices is in several hundreds of nanometer, the acceptable thickness range of the surface roughness of the flexible electrode needs to be within 100 nm.
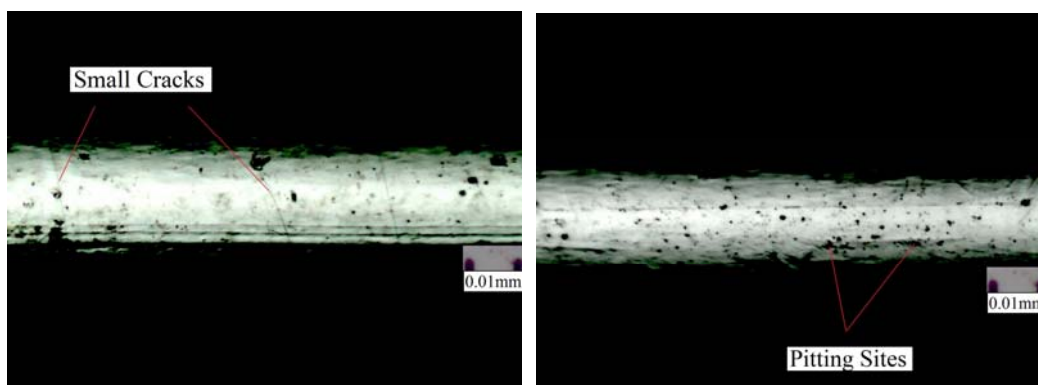
Figure 4.4   Small cracks (left) and pitting sites (right) on Ni-coated PET fibres (Pd=3min; Ni=3min) etched with 4M NaOH etching solution at 20℃ for 10 min

4.3.2   Surface morphology of the Ni-coated PET fibres due to process parameters

The surface morphologies of Ni-coated PET fibres fabricated by using different processing parameters of metallization except deposition time of Ni-plating bath were investigated by optical microscope. The optimal processing parameters of the metalization conditions in order to fabricate Ni electrode with least surface defects were identified by comparing the optical micrographs. Furthermore, the effects of these processing parameters on the surface roughness of the metal coating were also revealed from the micrographs.

The metallization conditions used in the study were as follows: the fibre samples were etched with NaOH solution of various concentrations (4M, 6M and 8M) at various temperatures ($20^\circ C$, $40^\circ C$ and $60^\circ C$) for different hours (2hr, 4hr, 6hr and 8hr). Then, the treated samples were immediately dipped into the Pd-activation bath for different times (1min, 3min, 6min and 10min) and finally into Ni-plating bath for 3 min. The change of processing parameters were grouped into three sections, where two sections were related to the surface etching and the last one was the deposition time of Pd-activation bath, and the results are summarized in the Figures 4.5 to 4.10.

4.3.2.1   Effects of NaOH etching time/Concentration of NaOH solution on surface

morphology

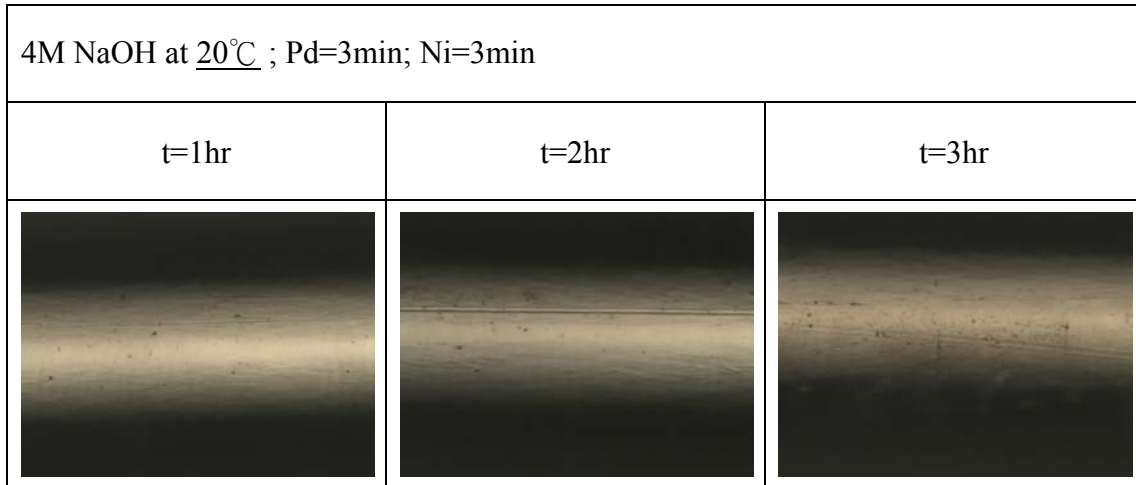| **4M** NaOH at 20℃ ; Pd=3min; Ni=3min			
t=2hr		t=4hr	
t=6hr		t=8hr	
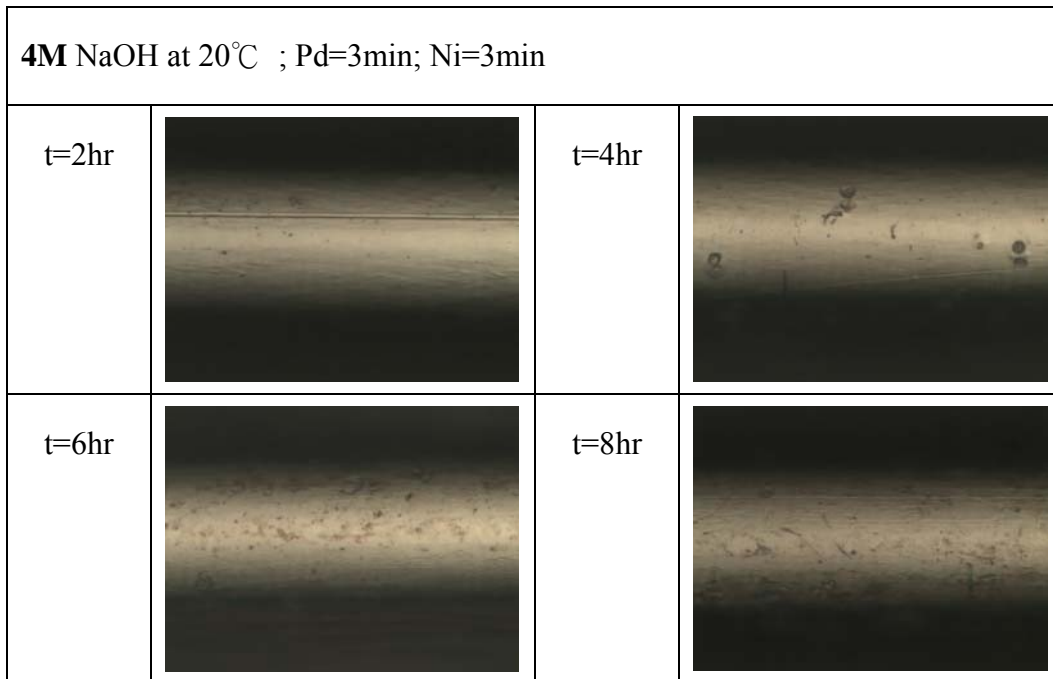
Figure 4.5   Optical micrographs of Ni-coated PET fibres etched with **4M** NaOH
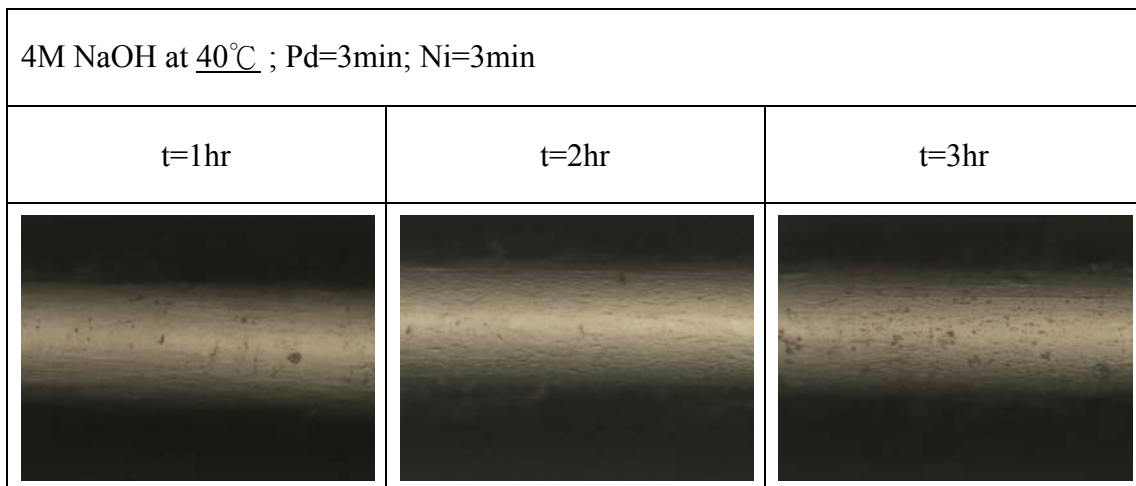
etching solution at 20℃ for various etching times

| **6M** NaOH at 20℃ ; Pd=3min; Ni=3min			
t=2hr		t=4hr	

| t=6hr | | t=8hr | |
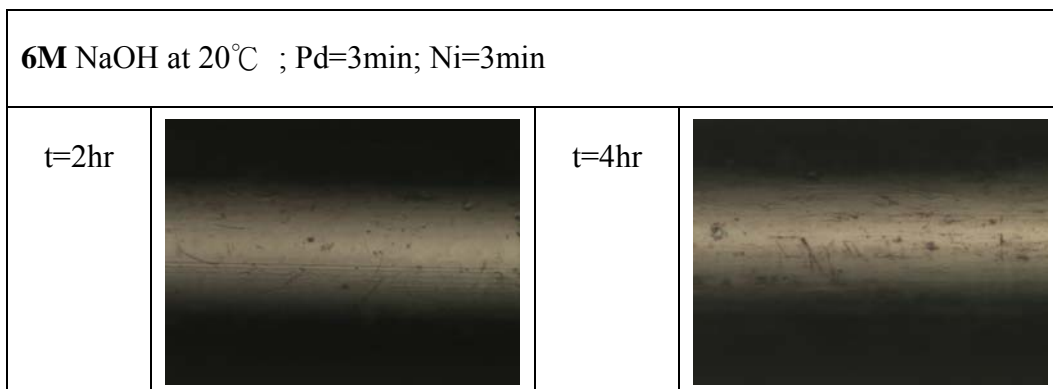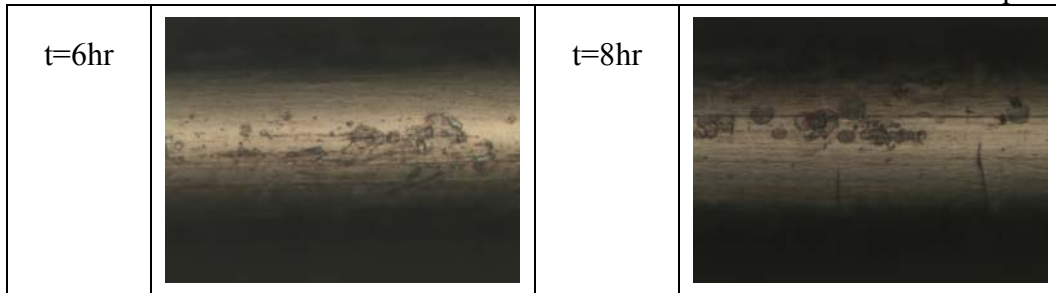
Figure 4.6 Optical micrographs of Ni-coated PET fibres etched with **6M** NaOH etching solution at 20℃ for various etching times

8M NaOH at 20℃ ; Pd=3min; Ni=3min			
t=2hr		t=4hr	
t=6hr		t=8hr	
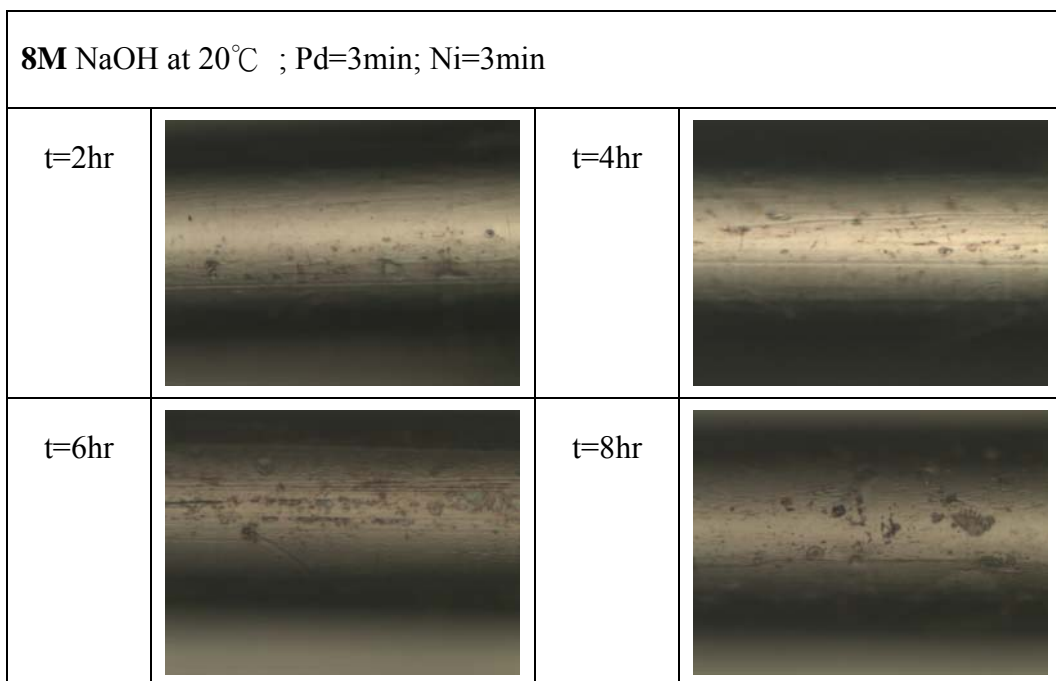
Figure 4.7 Optical micrographs of Ni-coated PET fibres (Pd=3min; Ni=3min) etched with **8M** NaOH etching solution at 20℃ for various etching times

The first section was to examine the effects of surface etching process including NaOH etching time and concentration of NaOH etching solution (Figures 4.5 to 4.7). This set of the PET fibres were etched in different concentration of NaOH solution at

20℃ using different etching times. The Pd-activation time and electroless Ni time were fixed at 3 min. Pitting sites of larger size and denser packing were formed on the surface of the PET fibres when the etching time was increased (Figures 4.6 and 4.7). Hence, the proper etching time was 2 hr. Besides etching time, this trend of getting larger and denser pitting sites was more evident at higher NaOH concentration. General speaking, surface with too many pitting sites (over-etching) occurred easily in high NaOH concentration, say 8M NaOH. This over-etching would certainly degrade the mechanical properties of the PET fibres, i.e. the fibres would become brittle and the surface would easily peel off even after metal coating had been grown on the PET surface. As a result, 4M NaOH solution was selected as the proper etching solution in order to have a better controlled etching process and create carboxylate ions (RCOO⁻ ions) which are essential for successive steps of the metallization process via hydrolysis of PET and reduce the probability of over etching.

4.3.2.2   Effect of NaOH etching temperature on surface morphology

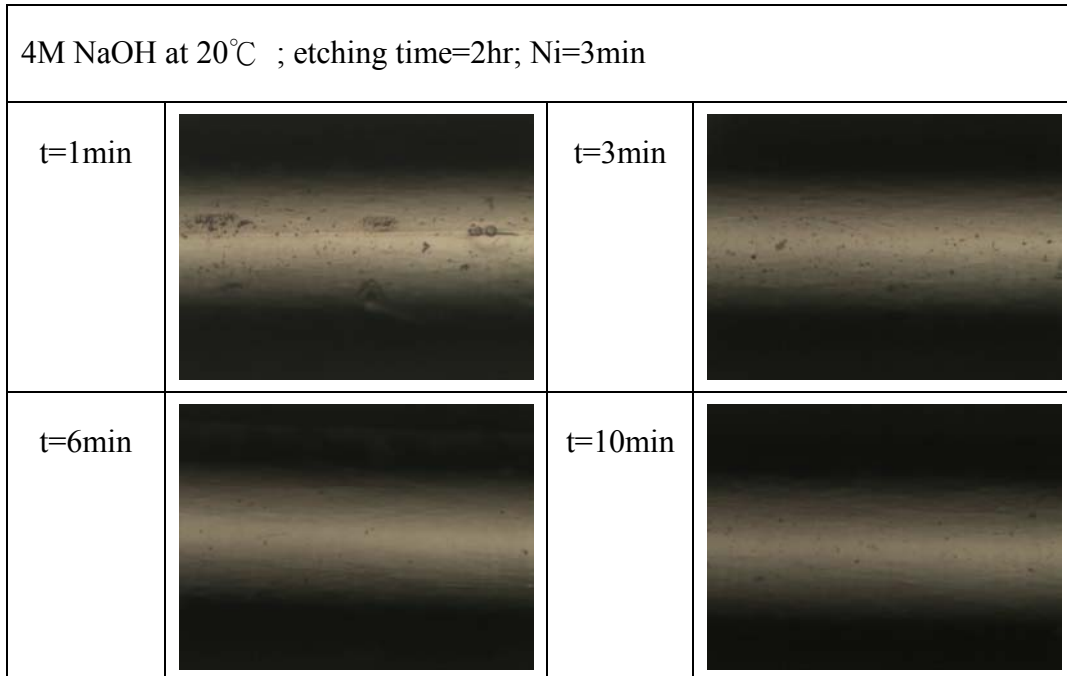| 4M NaOH at <u>20℃</u> ; Pd=3min; Ni=3min		
t=1hr	t=2hr	t=3hr

Figure 4.8   Optical micrographs of Ni-coated PET fibres etched with 4M NaOH etching solution at 20℃ for various etching times

4M NaOH at <u>40℃</u> ; Pd=3min; Ni=3min		
t=1hr	t=2hr	t=3hr

Figure 4.9   Optical micrographs of Ni-coated PET fibres etched with 4M NaOH etching solution at 40℃ for various etching times

4M NaOH at <u>60℃</u> ; Pd=3min; Ni=3min		
t=1hr	t=2hr	t=3hr
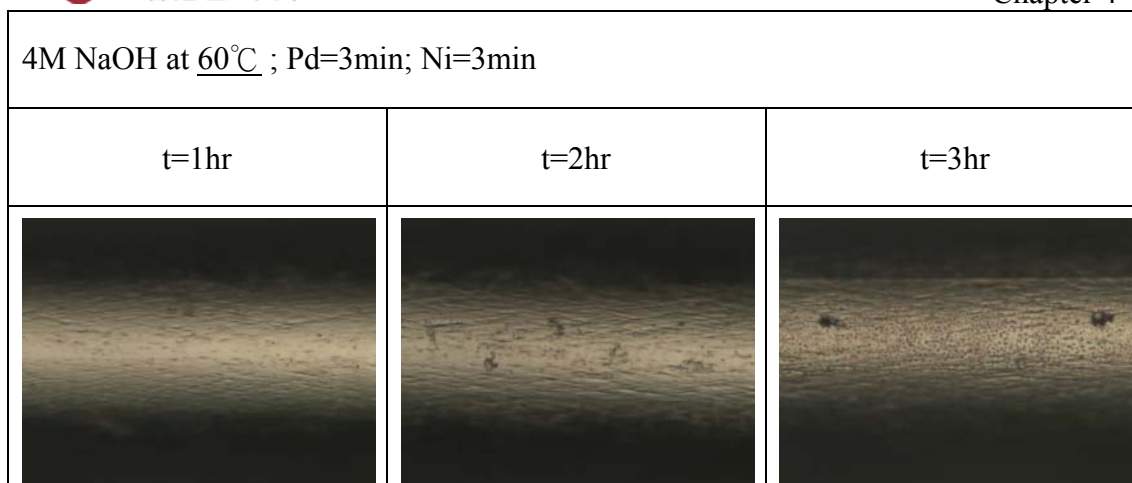
Figure 4.10   Optical micrographs of Ni-coated PET fibres etched with 4M NaOH etching solution at 60℃ for various etching time

The second section was to examine the effects of surface etching using different NaOH etching temperatures (Figures 4.8 to 4.10). Here, all the samples were etched in 4M NaOH solution. The etching time was narrowed from 1 to 3 hr. Stripe-like patterns of the Ni layer were formed on the fibre surface when the etching temperature increased from 20 to 60℃. The formation of the stripe-like patterns was more evident at higher etching temperature and longer etching time. Moreover, small and dense pitting sites increased in numbers with etching time at higher etching temperature, in particular, 60℃. Hence, the optimal temperature for the etching process was 20℃ so as to avoid the formation of stripe-like patterns on the Ni-coated PET fibres, in other words, in order to minimize the surface roughness of the electrodes.

4.3.2.3   Deposition time of Pd-activation

4M NaOH at 20℃ ; etching time=2hr; Ni=3min			
t=1min		t=3min	
t=6min		t=10min	

Figure 4.11   Optical micrographs of Ni-coated PET fibres etched with 4M NaOH etching solution at 20℃ for various deposition time of Pd-activation

The third section investigated the effects of deposition time of Pd-activation bath (Figure 4.11) on the surface morphology of the Ni-coating on PET fibres. This set of PET fibres were etched in 4M NaOH solution for 2 hr at 20℃ but processed with different Pd-activation time. As shown in Figure 4.11, at short Pd-activation time of 1 min, some pitting sites were formed on the surface of the fibres. As Pd-activation became longer above 3 min, no observable pitting site was detected. The surface morphology of the samples with Pd-activation times of 3 min, 6 min and 10 min

looked very similar, indicating that smooth Ni-coating without pitting sites could be obtained using Pd-activation time above 3 min.

Hence, due to the expansive cost of Pd-activation bath, the PET fibres treated with the surface modifications were preferable to dip in the Pd-activation bath for 3 min only.

4.3.3   Cross-sectional morphology of the Ni- and Cu-coated PET fibres

Cross-sectional morphology of the Ni- and Cu-coated PET fibres was characterized by SEM. Thin Ni layer and thick Cu layer coated on the fibres were fabricated using electroless plating and electro-deposition methods respectively. The thicknesses of the Ni layer and Cu layer, which mainly depend on the parameters of the deposition time of electroless Ni-plating and electro-deposition of Cu respectively. The cross-section SEM micrographs of the Ni-coated PET fibre and Cu-coated PET fibre are shown in Figure 4.12 and 4.13 and the relationships between the thickness of the Cu-coating and the Cu-plating time, the Ni-plating time as well as NaOH etching time are summarized in Table 4.1.
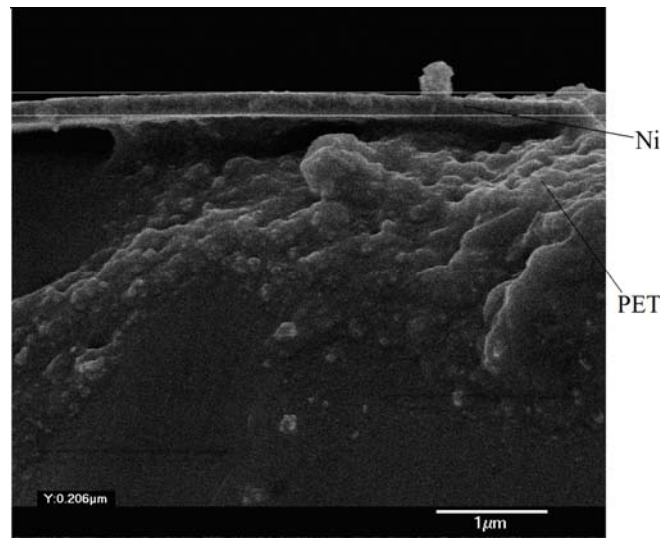
Figure 4.12   Cross-section of Ni-coated PET fibre (Ni-plating time=3 min)
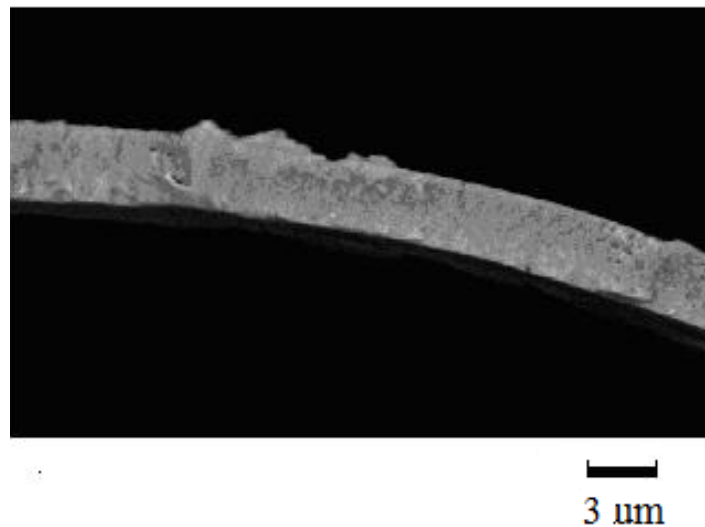
Figure 4.13   Cross-section of Cu-coated PET fibre (Cu-plating time=5 min)

According to Figures 4.12 and 4.13, the thicknesses of the Ni layer and Cu layer were found to be 206 nm and 3.15 μ m respectively. Both the metal coatings of Ni and Cu were illuminated to achieve uniform thickness deposited on the PET fibres.

Cu-plating time (min)	2	5	10	15
Thickness of Cu layer (μm)	1.64	3.15	7.24	20.71
Deposition rate (μm/min)	0.82	0.63	0.72	1.38

Table 4.1   Thicknesses of Cu-coated PET fibres with different Cu-plating time

General speaking, the thickness of the Cu layer increased as the Cu electroplating time increased. In the early stage of the electroplating, the resistance of the thin Ni layer was huge (further discussed on Section 4.3.4). This might result in a small current flowed through the sample. Then Cu ions in Cu-plating bath were supplied with fewer electrons to form Cu layer coated on the Ni layer. This obviously resulted in a relatively slow deposition rate. When the Cu layer became sufficiently thick (say 15 min), a large DC current of large amounts electrons flowed through the thick Cu layer due to the decrease of the resistance. Thus, more electrons were available for the reduction of Cu ions in the solution baths. Hence, the thickness of the Cu layer increased significantly in the case of 15 min deposition time.

Moreover, thickness of Ni layer due to different Ni-plating time was investigated using FE-SEM. The thickness of Ni layer increased with Ni-plating time as shown in Figure 4.14. Obviously, thicknesses of Ni layer increased with Ni-plating times.
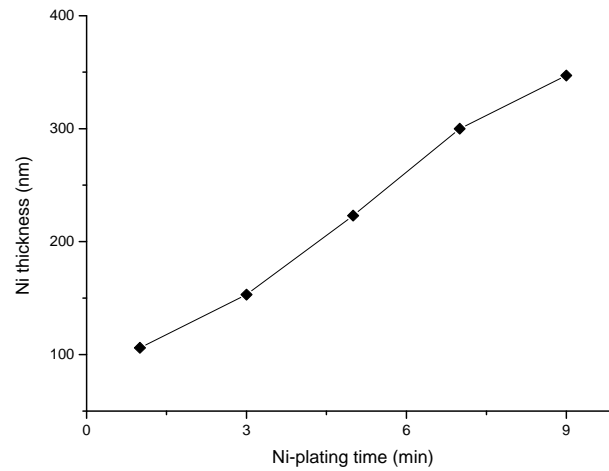
Figure 4.14   Thicknesses of Ni layer due to different Ni-plating time

4.3.4   Electrical measurement of the Ni-coated PET fibres

Electrical measurements of the Ni layer coated on the PET fibres were investigated using four-point probe method in order to eliminate impedance contribution due to wiring and contact resistances. The probes were equally spaced and the measurement was conducted at room temperature.

According to equation (2.3), correction factor was required to consider effects of electric current divergence (current flowing in all possible directions) due to different geometry. Since there was only one route for electric current to flow through the fibre, the current from a constant-current source was passed through the outer two probes and the fibre without divergence in current flowing. Hence, no correction factor was applied for this four-point probe measurement.

Resistivity measurement of the Ni-coated fibres with different Ni-plating times as well as surface etching times was conducted. Moreover, the effects of Ni-layer thickness and NaOH etching time on the resistivity were investigated. The corresponding I-V graphs were shown in Figures 4.15 to 4.17. The obtained resistivity and conductivity of the Ni-coated PET fibre for different Ni-plating and NaOH etching time are summarized in Table 4.2.
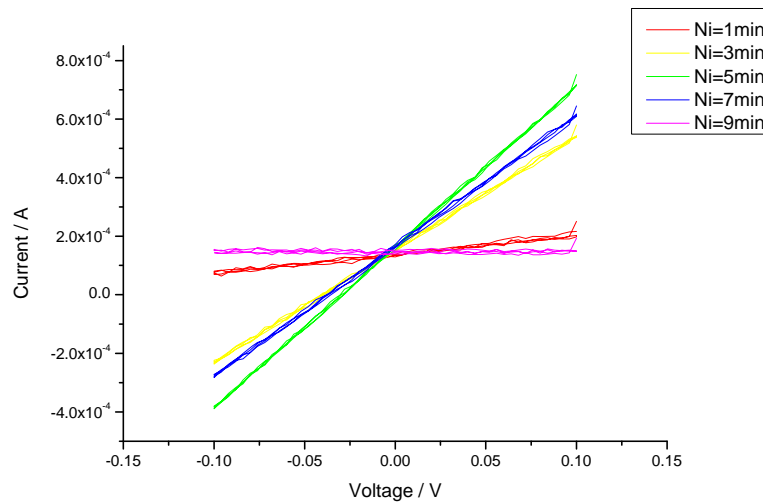
Figure 4.15   IV graphs of Ni-coated PET fibres with different Ni-plating time for same NaOH etching time of 10 min
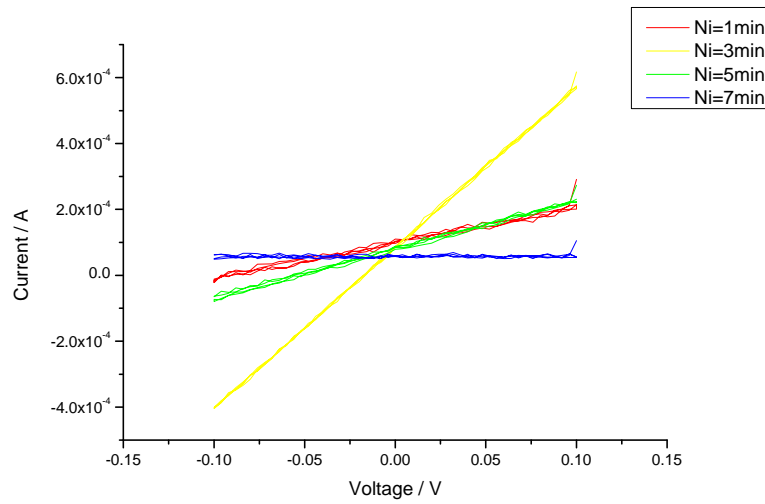
Figure 4.16   IV graphs of Ni-coated PET fibres with different Ni-plating time for

same NaOH etching time of 1 hr
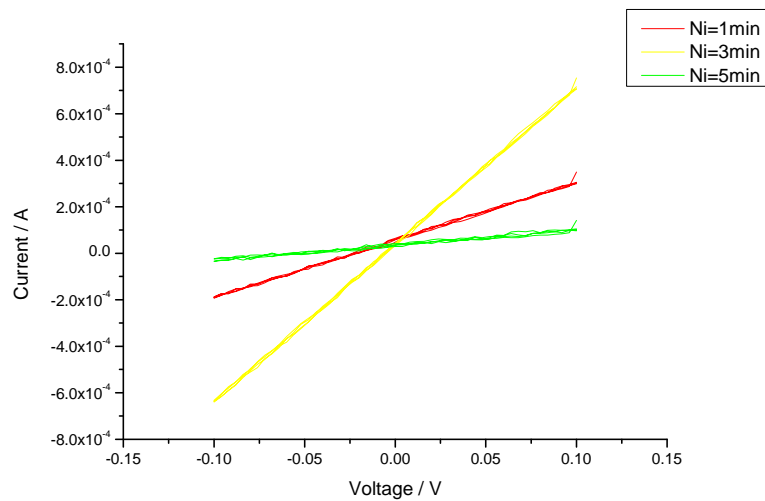
Figure 4.17   IV graphs of Ni-coated PET fibres with different Ni-plating time for

same NaOH etching time of 2 hr

Ni-plating time (min)	R (Ω)	t (nm)	ρ (Ω/m)	σ (S/m)
For etching time=2 hr,				
1	1.52E+03	106	1.61E-04	6.20E+03
3	2.56E+02	153	3.92E-05	2.55E+04
5	1.82E+02	223	3.75E-05	2.67E+04
7	2.27E+02	300	6.82E-05	1.47E+04
9	7.03E+05	347	2.44E-01	4.10E+00
For etching time=1 hr,				
1	9.09E+02	106	9.64E-05	1.04E+04
3	2.04E+02	153	3.12E-05	3.20E+04
5	6.67E+02	223	1.37E-04	7.28E+03
7	1.01E+05	300	3.02E-02	3.31E+01
For etching time=10 min,				
1	4.04E+02	106	4.28E-05	2.34E+04
3	1.47E+02	153	2.25E-05	4.44E+04
5	1.67E+03	223	3.43E-04	2.91E+03

Table 4.2   Resistivity and conductivity of the Ni-coated PET fibre for different

Ni-plating and NaOH etching times

The reciprocal of the slope was electrical resistance. Figures 4.15 to 4.17 indicated that ohmic Ni layer was successfully coated on the PET fibres. Based on the I-V characteristics, for fixed NaOH etching time (say 2 hr), the largest slope, in other words, the lowest resistance was Ni-plating time of 5 min. At shorter Ni-plating times such as 1 min, the thickness of the Ni layer was too thin which impedes the flowing of electric current; at long Ni-plating times such as 9 min, surface cracks were formed on the Ni layer which resulted in very large impedance. The large impedance caused measurement errors. Hence, negative slope of I-V graphs were observed in Figures 4.15 and 4.16. Similar trends were also observed for different NaOH etching times.

Besides, the effects of NaOH etching time on the conductivity were studied. Longer etching time resulted in a rougher surface which enhanced the scattering of electron. Thus, the resistance of the coating would be decreased with NaOH etching time. This can be observed in Table 4.2, in particular for Ni-plating times of 1 min and 3 min.

However, for longer Ni-plating time of 5 min, the trend seems to be revealed. This might be due to longer Ni-plating time of 5 min. The overall thickness of the Ni coating is very large and thus the roughness of the fibre became neglectable.

For Ni-plating times over 5 min, say 7 min or 9 min, the resistance of the samples increased substantially. This might be due to the cracks developed on the Ni coating, resulting in larger resistance.

Since NaOH surface etching provide rough surface to enhance implementation of Pd metal ions on PET substrate for better adhesion and reduce surface defects of the finished metal layers, in particular, electroless Ni layer, different etching times are believe not to affect the thickness of the Ni layer. The resistivity of the Ni layer (Ni-plating time=3 min) on top of the PET fibre was found to be ~10^{-5} Ω/m. Compared with the standard value of the resistivity of bulk Ni metal which is 6.99×10^{-8} Ω/m at 20℃,[38,39] the resistivity of the Ni layer had two orders of magnitude larger than the standard value. This was probably due to defects of the Ni layer and small fibre geometry.

4.4　Conclusion

Ni and Cu coatings on 3D circular PET fibres acting as the bottom electrodes for future flexible solar cell applications were successfully fabricated via a modified wet chemical technique for metallization. The PET fibres needed to be thermally bonded to a 2D planar PET sheet and then dipped together into sequential chemical baths for the corresponding metallization processes.

The effects of five metallization parameters including (a) concentration of NaOH solution, (b) etching time of the NaOH bath, (c) temperature of the NaOH bath, (d) deposition time of Pd-activation and (e) Ni-plating baths on the thickness, the surface

morphology and the conductivity of the Ni-coated PET fibres were investigated. Electrodes of good conduction, adhesion and flexibility could be obtained using appropriate metallization process parameters.

The thickness of the Ni and Cu layer was based on the deposition time of the treated PET fibre in the electroless Ni-plating and electro Cu-plating baths respectively. The typical thickness of the Ni layer was 206 nm (Ni-plating time=3 min), while that of Cu layer was 3.15 μm (Cu-plating time=5 min). Thickness of the Cu layer increased as the electro Cu-plating bath time increased.

The four-point probe measurement verified that the Ni layer was ohmic conductor. The resulting resistivity of the metal coating of Ni (Ni-plating time= 3min) was about 3×10^{-5} Ω/m, which was worse than the corresponding bulk value of the same material. It was probably due to the defects of the Ni layer and small fibre geometry.

Thickness of Ni layer increased with Ni-plating time. At Ni-plating time of 1min, the thickness of the Ni layer was too thin which impedes the flowing of electric current; at long Ni-plating time, surface cracks were formed on the Ni layer which lowered the electrical performance.

On the basis of our results, metallization conditions to achieve good Ni-coated PET fibres were that the samples should be etched with 4M NaOH solution at room temperature for 2 hr and the treated samples were immediately dipped in the

successive Pd-activation and Ni-plating baths for 6 and 3 min respectively. In this case, the Ni-coated fibres should possess good surface morphology as well as high conductivity.

CHAPTER 5   FABRICATION AND CHARACTERIZATION OF VERTICAL-ALIGNED ZINC OXIDE NANOROD ARRAYS ON METAL-COATED POLYESTER FIBRES

5.1 Introduction

5.1.1   Objective

In the third stage of the project, the objective is to fabricate vertical arrays of ZnO nanorod on metal-coated PET fibres via wet chemical routes. In this part, Ni layer was used as the metal layer. The reasons using Ni as the electrode were that Ni has a relatively good conductivity and the process to fabricate Ni-layer is quite easy and simple. These structures can be used for future photovoltaic application of hybrid inorganic nanorod/polymer solar cell.

5.1.2   Structure of ZnO nanorods grown on Ni-coated PET fibers

The schematic diagram of ZnO nanorod arrays grown on a Ni-coated PET fibre is shown in the following figure (Figure 5.1):
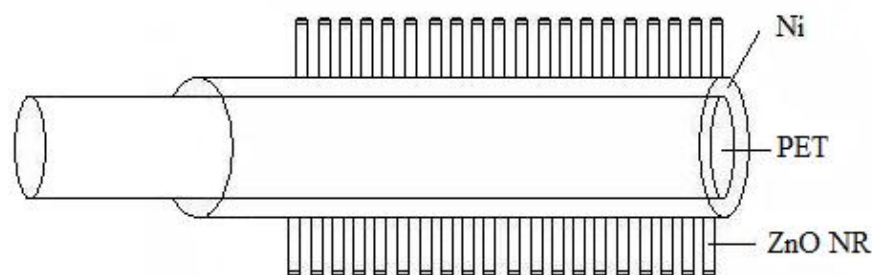
Figure 5.1   Schematic structure of ZnO NRs grown on Ni-coated PET fiber

Before growing ZnO nanorod array, a thin layer of Ni was deposited onto the PET fibre (T1203-1 #37) using electroless plating technique. The Ni-coated PET fibers with good electrical conductivity were used as bottom electrodes as well as substrates for the deposition of ZnO nanorods.

ZnO, a II-VI semiconductor, is intrinsically n-type and has excellent electrical as well as optical properties. The vertical alignment of the nanorods provides advantageous flexibility and direct path for charge transport. Indeed, vertical-aligned ZnO nanorods had been reported to be a promising candidate for flexible solar cell applications.[40-43] The ZnO nanorods, intrinsically working as n-type material, were deposited onto these fibers by chemical solution deposition (CBD) technique.

5.2 Methodology

5.2.1 Fabrication method - Chemical Bath Deposition

The Ni-coated polyester fibers as well as sheets were first fabricated by electroless nickel plating method. The processing parameters for the Ni-coated PET fibres were the followings: the concentration of NaOH used was 4M, the etching time of NaOH was 2 hr, the Pd activation time was 3 min, and the electroless Ni-plating time was 3 min. Based on these processing conditions, the thickness of the Ni-coating was about 200 nm. After that, aqueous solutions of zinc nitrate hexahydrate ($Zn(NO_3)_2 \cdot 6H_2O$) and hexamethylenetetramine (HTMA) of concentration 0.058 g/ml and 0.028 g/ml respectively,[44] were mixed together in a beaker. The beaker was placed in a water bath to maintain at a constant temperature of 95℃. Similar to the fabrication of Ni-coating on PET fibres, the Ni-coated PET fibres were also thermally bonded to a Ni-coated PET sheet or a transparent PET sheet. The polyester sheet and the fibres were dipped into the chemical bath as shown in Figure 5.2. As the chemical solution had a relatively high density, the PET substrate floated on the surface of the solution. In order to make sure the ZnO nanorods growing on the PET fibres, the surface of the sheet bonding with the fibres had to be faced down. The deposition time for the growth of ZnO nanorods on the Ni-coated PET fibres was fixed at either one hour or three hours.
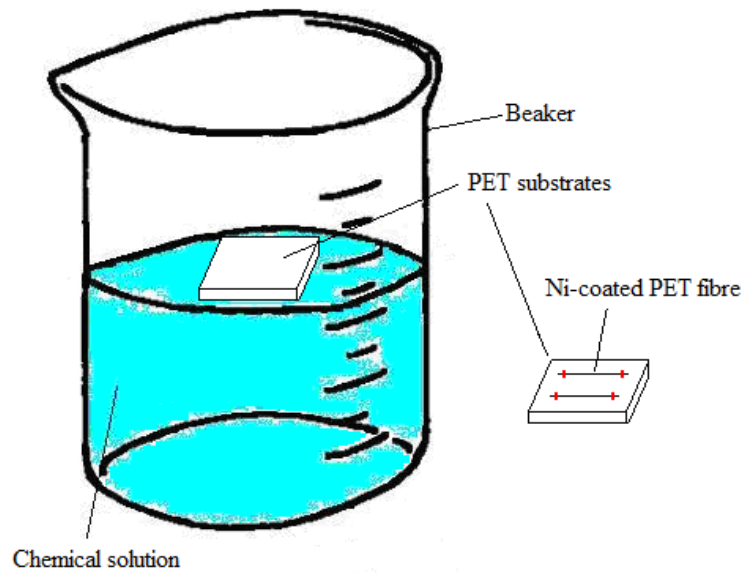
Figure 5.2　Schematic diagram of the PET substrates placed in the beaker

Besides the direct growth of ZnO nanorods onto Ni-coated PET fibres using CBD, a thin ZnO seed layer was first deposited onto the Ni-coated PET fibres using pulsed laser deposition (PLD) technique. After that ZnO nanorod array was deposited onto the ZnO seed layer. This additional seed layer improved the vertical alignment of the ZnO nanorods on the Ni-coated polyester fibres.

5.2.2　Characterization methods

The structural and optical properties of the ZnO nanorods grown on Ni-coated PET fibres as well as ZnO seed-layer/Ni-coated PET fibres had been characterized. For the structural characterization, the structural phases of the ZnO nanorods were studied by using XRD and Raman scattering. X-ray diffraction (XRD) measurement was

performed using θ-2θ configuration and Raman scattering was conducted using a micro-Raman spectroscope with excitation wavelength of 488 nm. The surface and cross-section morphologies of the ZnO nanorods were examined using field-emission scanning electron microscope (FE-SEM).

For the optical characterization, room-temperature transmittance measurement of the ZnO nanorods grown on uncoated PET sheet was performed using UV-Visible spectrophotometer. Photoluminescence measurement was also conducted using Nd:YAG laser with excitation wavelength of 266 nm at pulsed operation(10 Hz, 6 ns).

5.3 Results and discussion

In growing ZnO nanorods, different substrates had been used. They included uncoated PET sheets, Ni-coated PET fibres and Ni-coated PET fibres with a PLD-derived ZnO seed layer. The main purpose of using uncoated PET sheet as substrate to grow ZnO nanorods was that this sample allowed us to measure the transmittance spectra as well as XRD of the ZnO nanorods. For the two different types of fibre, namely, with and without the PLD-derived ZnO layer, we would try to reveal the effects of the ZnO template layer on the growth of ZnO nanorods. Besides different substrates, two different deposition times for the ZnO nanorods, namely one hour and three hours, were also used.

5.3.1   SEM images of ZnO nanorods on different substrates

5.3.1.1   ZnO nanorods grown on uncoated PET sheet

The ZnO nanorods were fabricated on PET sheet by dipping into the solution consisting of the two precursors with appropriate concentration. Vertically-aligned ZnO nanorods without impurities were successfully formed on the pure PET sheet under the experimental conditions of deposition temperature of 95℃ and deposition time of three hours. The SEM micrographs showing the surface morphology of the nanorods are displayed in Figures 5.3 (a) and (b).
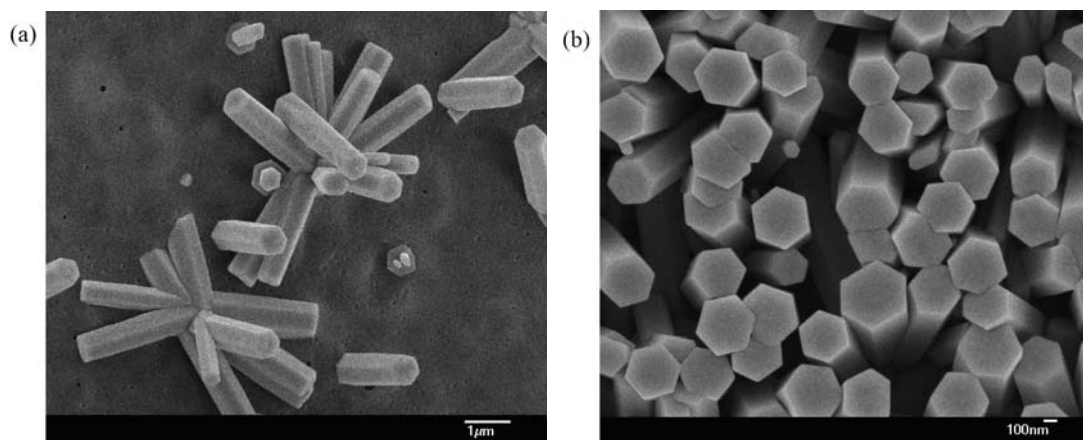
Figure 5.3   Surface morphology of ZnO nanorods grown on non-coated PET sheet (deposition time=3 hr)

As shown in Figure 5.3 (a), the formation of the ZnO nanorods was random and non-uniform. Some parts of the sheet had the ZnO nanorods while some parts did not

have. In additional, the orientation of the ZnO nanorod arrays was slightly random which might cause random path for charge transport. Figure 5.3 (b) shows a close look of a selective ZnO nanorod array. Clearly, ZnO nanorods had a characteristic hexagonal form with about 1.75 μ m in length and 450 nm in diameter as shown in Figures 5.3 (a) and (b) respectively.

5.3.1.2 ZnO nanorods grown on Ni-coated PET fibres

Same experimental conditions for the growth of ZnO nanorods on pure PET sheet were applied in the fabrication of ZnO nanorods on Ni-coated PET fibres. The SEM micrographs showing the surface morphologies of the ZnO nanorods on Ni-coated PET fibers with different deposition times are shown in Figures 5.4 and 5.5. Here, deposition time of one hour and three hours were employed and they were denoted as sample A and sample B respectively.
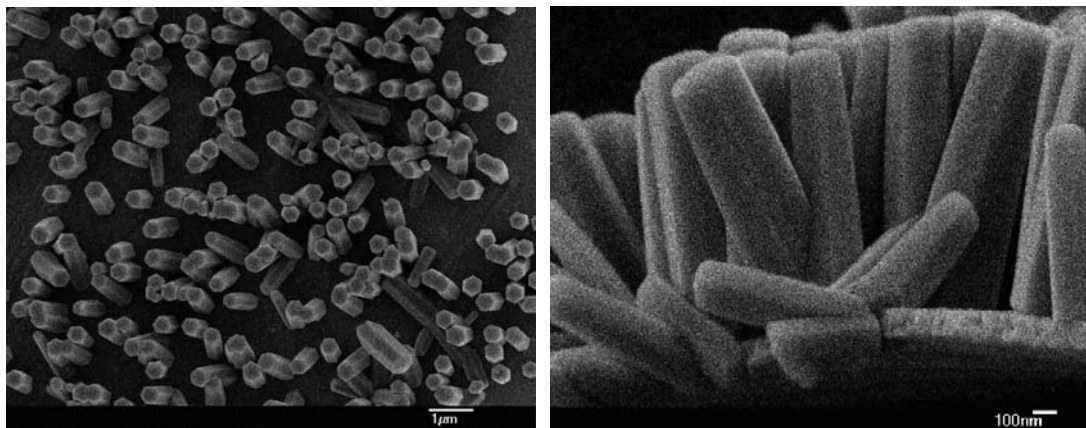
Figure 5.4 Surface (left) and cross-section (right) of ZnO nanorods on the fibres (Sample A, deposition time=1 hr)
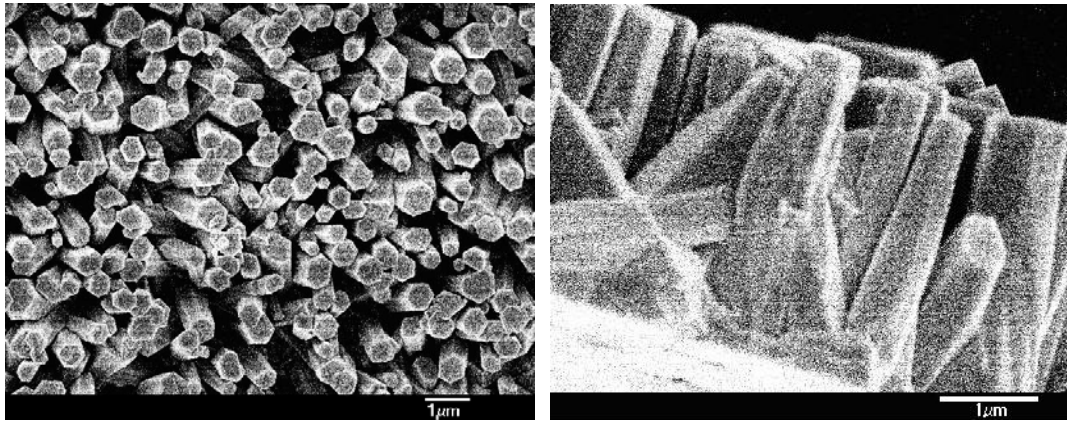
Figure 5.5 Surface (left) and cross-section (right) of ZnO nanorods on the fibres (Sample B, deposition time=3 hr)

Based on the SEM micrographs, vertical-aligned ZnO NRs were shown to be successfully deposited on top of the Ni-coated PET fibres. The thickness of the Ni layer was about 150 nm. In Figure 5.4, the ZnO nanorods were $1\,\mu$ m in length and 300 nm in diameter, whereas in Figure 5.5, the nanorods were $2\,\mu$ m in length and 500 nm in diameter. The aspect ratios (length-to-width ratio) of the ZnO nanorods grown on the Ni layer were between three and four for both deposition times of one hour and three hours. Besides, the packing density of the ZnO nanorods was different for different deposition time. Sample B was observed to have denser ZnO nanorod arrays

than that of sample A. Longer deposition time resulted in a denser, better-packed and more uniformly growth of ZnO nanorods. The size of the individual ZnO nanorod also increased with deposition time, in both the length as well as the diameter. However, the aspect ratio remained around three to four which was close to value obtained at shorter deposition time. Therefore, for deposition of one to three hours, the aspect ratios are more or less the same. This result suggested that the aspect ratio does not affected by the deposition time between one to three hours.

For the same deposition time of three hours, the diameters and lengths of the ZnO nanorods grown on the Ni-coated fibre and uncoated PET sheet were found to be 500 nm and $2\,\mu$m, and 450 nm and $1.75\,\mu$m respectively, i.e. they both had similar diameters and lengths for ZnO nanorods. The aspect ratio was close to four and seemed not related to the substrate very much. However, a large difference in the growth density of nanorods was observed. In the Ni-coated fibre, the ZnO nanorods were denser and uniformly grown on the surface. Thus, our results demonstrated that the size and aspect ratio of the ZnO nanorods were not affected very much by the substrates. Indeed, the growth density of the ZnO nanorods was strongly influenced by the substrates. In our experiments, our results indicated that the Ni layer seemed to assist the growth of ZnO nanorods, resulting in a more uniform and evenly distributed ZnO nanorod arrays on the PET surface.

5.3.1.3   ZnO nanorods on Ni-coated PET fibres with the addition of ZnO seed layer

The ZnO nanorods were also grown on the Ni-coated PET fibre with a thin ZnO seed layer to achieve continuous layer growth. A thin ZnO seed layer (approximately 20 nm) was deposited onto the Ni-coated PET fibre using pulsed laser deposition (PLD) technique before the growth of ZnO nanorods. In the PLD experiment, a pure ZnO target was used. The excimer laser was operated at an energy density of 1.88 J/cm^2 and a repetition rate of 10 Hz. The oxygen-filled chamber was kept at a constant pressure of 20 mTorr during the deposition. The substrate temperature was fixed at room temperature and the deposition time was 2 min. During the growth, the fibre was rotated slowly to make sure the ZnO seed layer was uniformly formed on the whole surface of the fibre.

After that, the ZnO nanorods were grown on the treated fibres using CBD with a deposition time of one hour. All the deposition conditions were remained the same as those in the fabrication of ZnO nanorods grown on PET sheets as well as Ni-coated PET fibres. The SEM micrographs showing the surface and cross-sectional morphologies of the ZnO nanorods grown on top of the thin ZnO seed layer/Ni-coated PET fibre structure is shown in Figure 5.6.
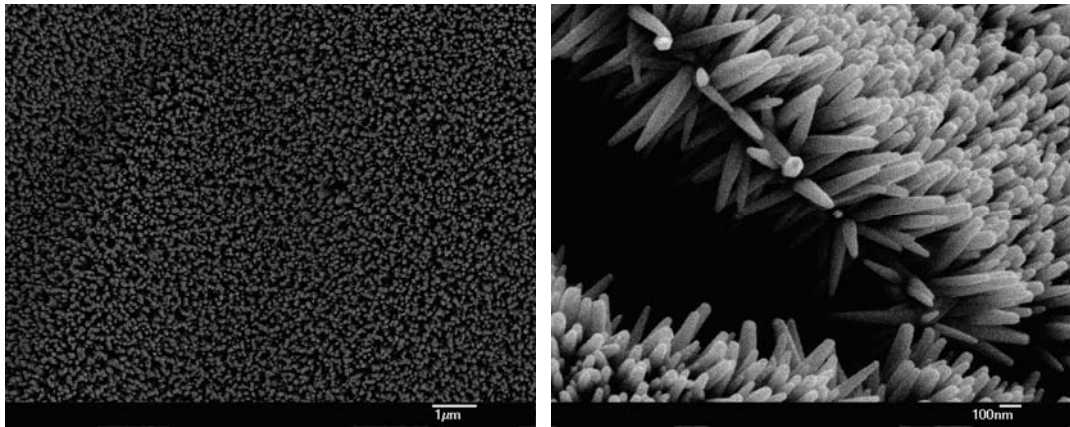
Fig. 5.6 Surface (left) and cross-section (right) of ZnO nanorod arrays with the addition of ZnO seed layer (deposition time=1 hr)

According to Figure 5.6, uniformly growth of vertical-aligned ZnO nanorod arrays on the Ni-coated PET fibre could be achieved due to the introduction of the ZnO seed layer in between the Ni layer and ZnO nanorod layer. Obviously, the introduction of ZnO seed layer favored the growth of ZnO nanorods. Compared to Figure 5.4, the ZnO nanorods grown on ZnO seed layer were observed to be densely packed with a smaller diameter and shorter length. Due to the packing density is much higher, the ZnO nanorods looked more uniformly distributed on the Ni-coated PET fibres with a ZnO seed layer. The diameters and lengths of the ZnO nanorods grown on the Ni-coated fibre and the ZnO seed layer/Ni-coated PET fibre structure were found to be 300 nm and 1000 nm, and 100 nm and 300 nm respectively under same deposition condition of one-hour deposition time. That means the aspect ratios of the ZnO

nanorods grown on the ZnO seed layer/Ni layer and Ni layer were around to be three to four. As a result, the aspect ratio was not likely to be affected by the substrate. This result is consistence with our previous observation.

Compared to the Ni-coated layer, the ZnO seed layer provided a better growing site for the formation of ZnO nanorods. A denser and more uniform-distributed ZnO nanorod array was obtained. However, the growth rate of the ZnO nanorods was slower in the ZnO seed layer/Ni-coated fibres than that in the Ni-coated fibres. The difference in the growth rate of ZnO nanorod on different layers could be explained by the competition between neighboring nanorods in addition to the preferential growth axis of the underlying layer.[45] The nucleation density on the seed layer was higher than that on the Ni layer. The high nucleation density provided a small volume of growth solution available for each nanorod which restricted the out-of-plane growth of the nanorods. Hence, shorter nanorods were obtained on the ZnO seed layer. Besides, at lower nucleation densities, the lateral growth was not effectively suppressed, resulting in nanorods of larger diameter grown the Ni layer.

During the CBD process, cracks were created when the Ni-coated PET fibres were dipped into the chemical solutions with a constant temperature of $95℃$. The possible reason was due to large mismatch of the thermal expansion coefficient of the 200 nm-thick Ni layer and the PET fibre substrate. The forming of the large cracks (as

shown in Fig. 5.6) limits the application of these ZnO nanorods fabricated on PET fibres.

5.3.2 XRD patterns of ZnO nanorods on Ni-coated PET sheet

X-ray diffraction patterns of ZnO nanorods on Ni-coated PET fibre as well as on ZnO seed-layer/Ni-coated PET fibre were very weak and difficult to be obtained. Hence, ZnO nanorods grown on Ni-coated PET sheet using the same conditions of CBD method were used to perform the structural characterization. Theta–2-theta scan of XRD was used to investigate the crystal structure of ZnO nanorods prepared on the Ni-coated PET sheet. Figure 5.7 shows the XRD pattern of ZnO nanorods grown on Ni-coated PET sheet. The deposition time used was one hour. Similar XRD pattern also obtained for ZnO nanorods grown on Ni-coated PET sheet with deposition time of three hours. Therefore, the crystal structure of ZnO nanorods in samples with different deposition times was almost the same.
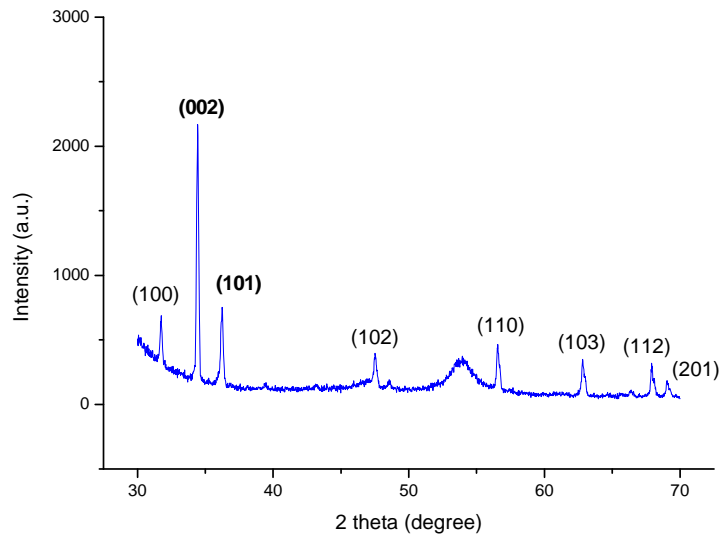
Figure 5.7   XRD patterns of the ZnO nanorods grown on Ni-coated PET sheet (deposition time=1 hr)

In Fig. 5.7, the location of the diffraction peaks of the ZnO nanorods matched with those reported diffraction peaks of ZnO bulk materials in between the 2-theta range of $30°$ and $70°$. Generally, strongest XRD peak of hexagonal ZnO film was arisen from the lattice plane (101).[Appendix B] In our sample, the dominating diffraction peak was located at $34.4°$ which referred to lattice plane (002). The dominating (002) diffraction peak indicated that highly c-axis oriented crystalline nanorods were obtained. Hence, highly vertical-aligned ZnO nanorods whose deposition times of one hour and three hours could be verified from the XRD patterns. This was consistence with the SEM results.

5.3.3　Raman spectra of ZnO nanorods on Ni-coated PET sheet and fibre

Micro-Raman measurements of the ZnO nanorods grown on the Ni-coated PET sheet and Ni-coated PET fibre were conducted at room temperature in a backscattering geometry using a HR-800 model spectrometer. The excitation source was 488 nm from an Argon-ion laser. The Raman spectra ranging from 100 to 1500 wave-number were displayed in Figure 5.8 and 5.9.
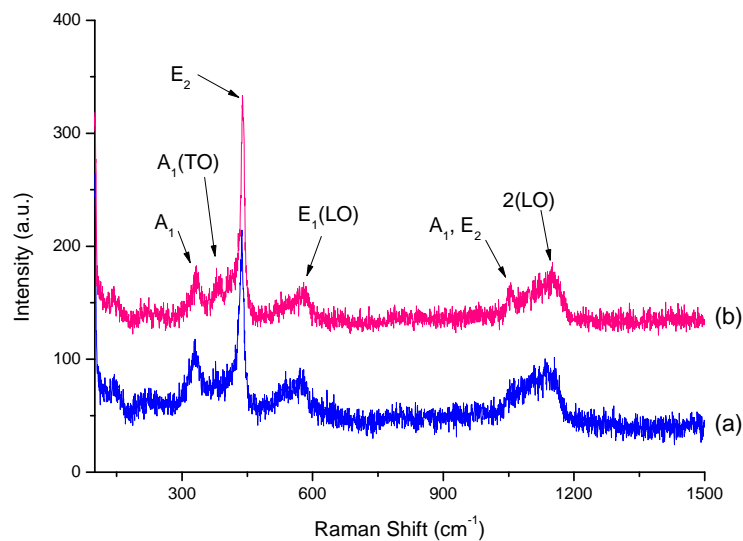
Figure 5.8　Raman spectra of ZnO nanorods : (a) grown on Ni-coated PET sheet (deposition time=1 hr) (b) grown on Ni-coated PET fiber (deposition time=1 hr).
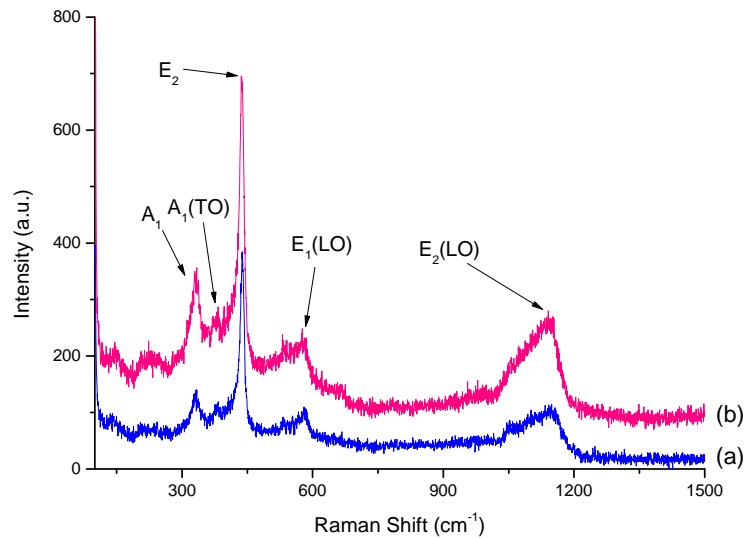
Figure 5.9   Raman spectra of ZnO nanorods : (a) grown on Ni-coated PET sheet (deposition time=3 hr), (b) grown on Ni-coated PET fiber (deposition time= 3 hr).

Sharp phonon peaks of the ZnO nanorods located at wave-number of 332, 436, 584 and 1153 cm^{-1} were clearly observed in the Raman spectra. The phonon peaks represented the vibrational modes of the ZnO nanorods. There were four sharp peaks and two weak peaks in the Raman spectra. From literature review of the Raman spectra of bulk ZnO,[46, 47] the sharp peak at 331 cm^{-1} was assigned as the A_1 symmetry mode, while the peak at 436 cm^{-1} was attributed to ZnO non-polar optical E_2 phonon. The peaks at 584 and 1154 cm^{-1} were LO and 2LO phonons of E_1 symmetry respectively. Besides, the weak peak at 383 cm^{-1} corresponded to the TO phonon of A_1 symmetry. The peak at 1101 cm^{-1} was the phonon mode of A_1+E_2

symmetry. The location of the phonon peaks in our ZnO nanorod samples matched with these from the literature review.

Therefore, the Raman spectra together with the XRD patterns indicated that high-quality ZnO nanorods were obtained on Ni-coated PET sheets as well as the Ni-coated PET fibres.

5.3.4　Transmittance spectra of ZnO nanorods on transparent PET sheet

As remarked in Section 2.4.1, optical transmittance measurement can be used to determine the bandgap energy of semiconductor materials. Hence, optical transmittance measurement was used to determine the bandgap energy of the ZnO nanorods grown on transparent PET sheet. The room-temperature transmittance measurement was done in a wide range of wavelengths between 380 and 750 nm (the visible spectrum). The transmittance spectra of ZnO NRs were illuminated in Figure 5.10.
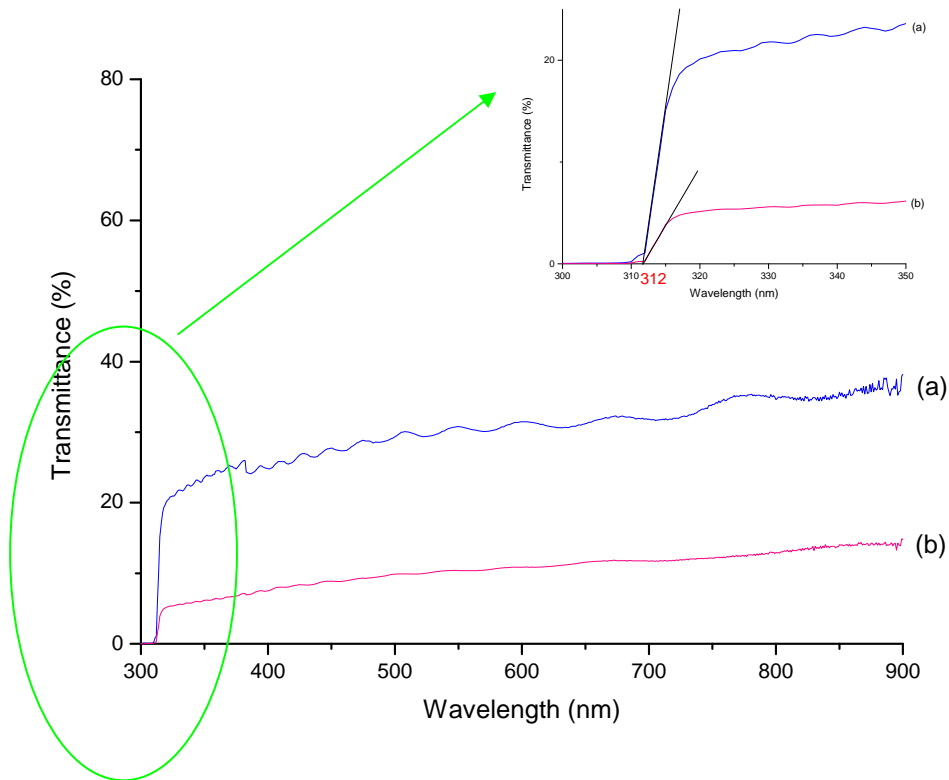
Figure 5.10   Transmittance spectra of ZnO NRs grown on transparent PET sheet

with deposition time of (a) 1 hr and (b) 3 hr. Straight lines: curve fitting for the two

samples.

Based on the transmittance spectra, ZnO nanorods have decreasing optical

transmittance with increasing deposition time. The transmittance of the samples were

approximate 30% and 10% at about 900 nm wavelength for samples with deposition

times of one hour and three hours respectively. This result is consistence with our

SEM micrographs. For longer deposition time, the packing density was much higher.

In addition, the ZnO nanorods were also longer, i.e. the equivalent layer thickness was

thus larger. We expected that the transmittance would be smaller. For each spectrum,

the transmittance decreased with wavelength which meant more light was absorbed

when approached to UV region. In the region of strong absorption, the transmission

decreased drastically to zero at the wavelength of 312 nm. Based on our

measurements, the two samples gave a similar value of 312 nm.

As mentioned in Section 2.4.1, the transmittance spectra was converted to the graph

of square of the optical absorption against photon energy ($\alpha(E)^2$ versus E) in order

to obtain value of bandgap energy of the ZnO nanorods through extrapolation the

linear part of the measurement to zero. The absorption profiles and the extrapolation

were shown in Figure 5.11.
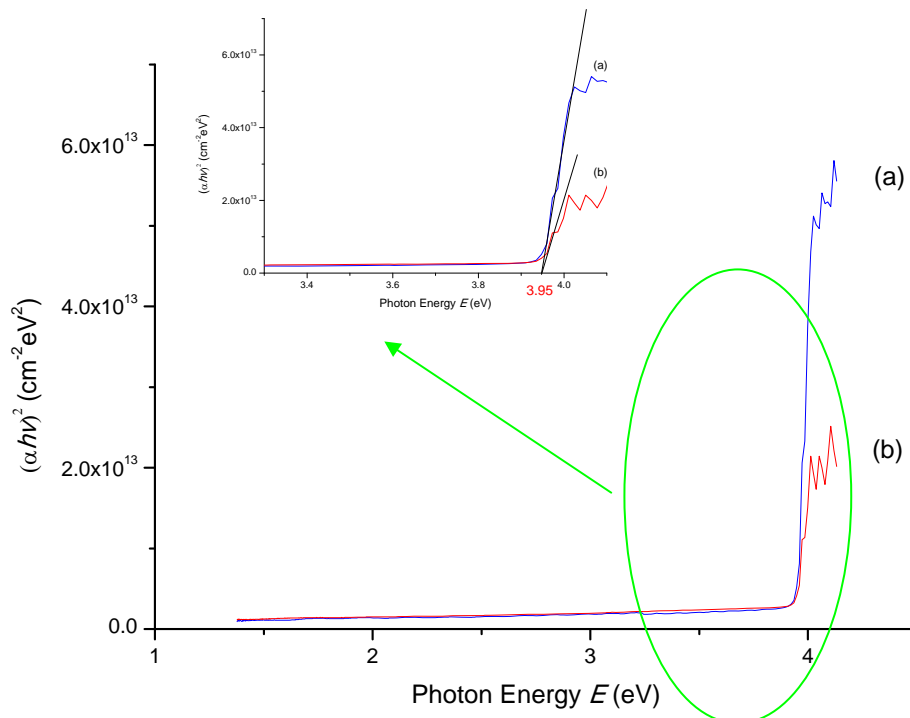
Figure 5.11 Absorption profiles of ZnO NRs grown on transparent PET sheet with

deposition time of (a) 1 hr and (b) 3 hr. Straight lines: curve fitting for the two

samples.

The transmission experiment has shown that the bandgap of ZnO nanowires is 3.9eV and this value is changed with the size of ZnO nanowires' diameter. However, it may be due to the influence of the void in the ZnO nanorod array causes the overestimated of bandgap.

According to Figure 5.11, the obtained bandgap energy of the ZnO nanorods was estimated to be 3.95 eV, by extrapolating the linear part of the graphs to zero in the region of strong absorption. As shown in Figure 5.11, both samples gave a similar bandgap energy. Literally, bulk ZnO has a band gap of 3.37 eV at room temperature, which corresponds to emission in the UV region.[15] The bandgap value of the ZnO nanorods was larger than the reported bulk value. The ZnO nanorod size for one-hour deposition time was 100 to 300 nm in diameter and few hundred nm in length. It is well known that the ZnO exciton binding energy is very large and consequently the exciton Bohr radius is only a few nm,[48] thus the nanorod size of 100nm is too big to see quantum size effect. The overestimated of bandgap value may be due to the influence of the void in the ZnO nanorod array.

5.3.5 Photoluminescence spectrum of the ZnO NRs on pure PET sheet

Photoluminescence (PL) characteristics of the ZnO nanorods grown on Ni-coated PET sheet were studied under optical excitation using a 266 nm Nd:YAG laser with an intensity of 10 mW. The laser offered out-of-plane excitation and emission of the vertical-aligned ZnO nanorods was detected as illuminated in Figure 5.12. The emission spectra of the ZnO nanorods grown on Ni-coated PET sheet with deposition times of one hour and three hours were shown in Figure 5.13.
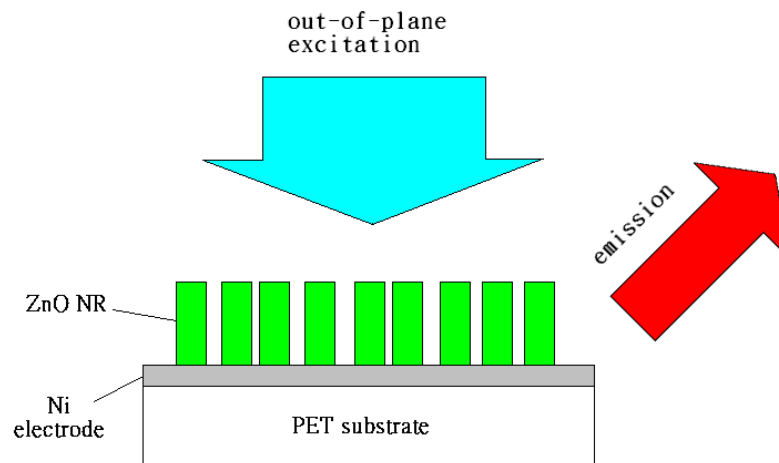
Figure 5.12   Schematic diagram of the PL measurement
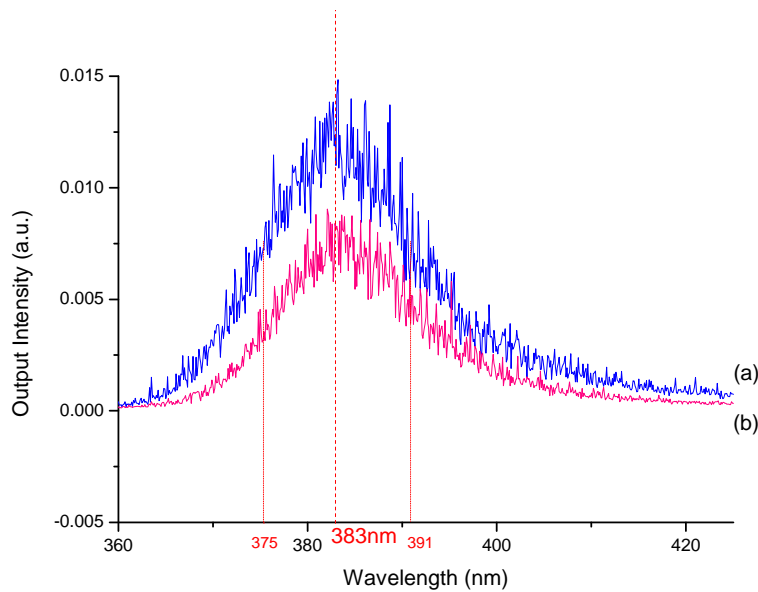
Figure 5.13   PL spectra of the ZnO nanorods grown on Ni-coated PET sheet with

deposition times of (a) 1 hr and (b) 3 hr

In the PL spectra, the peak position of the emission of both samples was at 383 nm.

The vertically aligned ZnO nanorods was excited from ultraviolet laser source of λ

=266 nm and released emission of λ =383 nm. The emission spectra indicated that

no free excitonic stimulated recombination was sustained because no other sharp

peaks were emerged from the spectra.[49] Both spectra had a similar full-width at

half-maximun (FWHM) of about 16 nm. Hence, same emission and FWHM were

obtained from the ZnO nanorods of different deposition times. Photoluminescence of

the ZnO nanorods was independent of deposition times, in other words, the size of the

nanostructure.

5.4 Applications

5.4.1   p-CZTS/i-CdS/n-ZnO thin film junction solar cell

Thin film technologies reduce the amount of material required for synthesis of active materials used in solar cell and provide flexibility on PV devices. Copper indium gallium selenide ($CuIn_{1-x}Ga_xSe2$ or CIGS) is one of promising semiconductor materials for thin-film technologies that are often used as outdoor PV applications. However, indium (In) and selenium (Se) are rare, so CIGS material is not a good option for large scale PV applications. Compared to $I-III-VI_2$ (CIGS) family, copper zinc tin sulfide (Cu_2ZnSnS_4 or CZTS) are cheaper in material cost because of abundant and nontoxic raw materials. CZTS has a near-optimum direct band gap energy of ~1.5 eV and a large absorption coefficient ($>10^4$ cm^{-1}). The theoretical limit of convection efficiency for CZTS is 32.2%.[50]

In order to demonstrate the application of the ZnO nanorods, we have fabricated a thin film p-i-n junction solar cell of CIGS-like structure (Figure 5.14) which used p-type CZTS nanoparticles to replace the p-type CIGS film in traditional CIGS-based solar cell. For the solar cell, n-type ZnO thin film of 200 nm in thickness was deposited on commercial ITO glass substrate using filter cathodic vacuum arc (FCVA) technique using deposition temperature of 100℃, pressure of 42 mTorr and deposition

time of 20 min. A 50 nm-thick cadmium sulfide (CdS) film was deposited on top of the ZnO film as buffer layer using chemical bath deposition. The function of the CdS layer was to improve interface properties and increase photon absorption.[51] The i-layer of CdS was as thin as about 50 nm in order to achieve good optical transmission. After that, p-type CZTS nanoparticals were deposited on the surface of the CdS layer by drop casting method. Al electrode was further patterned on the CZTS nanoparticls using thermal evaporation. In this structure, the incident sunlight illumines on the side of the ITO glass. Eventually, the same structure will be applied on the flexible PET substrate but using a transparent top electrode instead of Al electrode for real application.
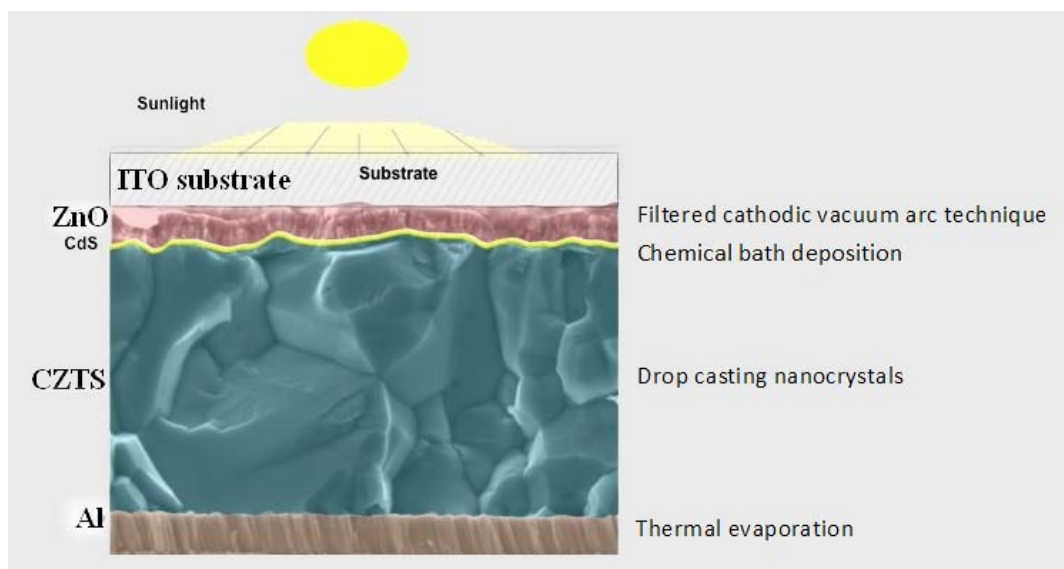
Figure 5.14   Schematic structure of CIGS-like p-i-n junction solar cell

The structural properties of this structure were characterized using XRD and SEM.

Their XRD diffraction patterns and SEM micrographs are displayed in Figures 5.15

and 5.16 respectively.
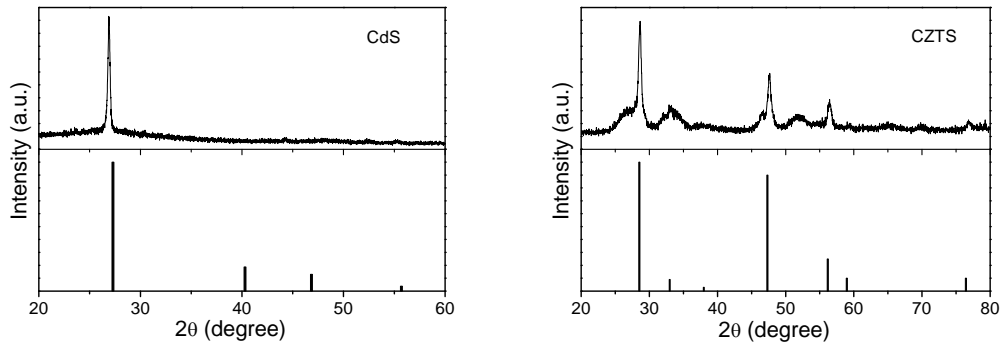
Figure 5.15   XRD patterns of CdS film [52] (left) and CZTS nanoparticles [53] (right).

The bottom parts of the XRD patterns were the peak positions obtained from

reference.
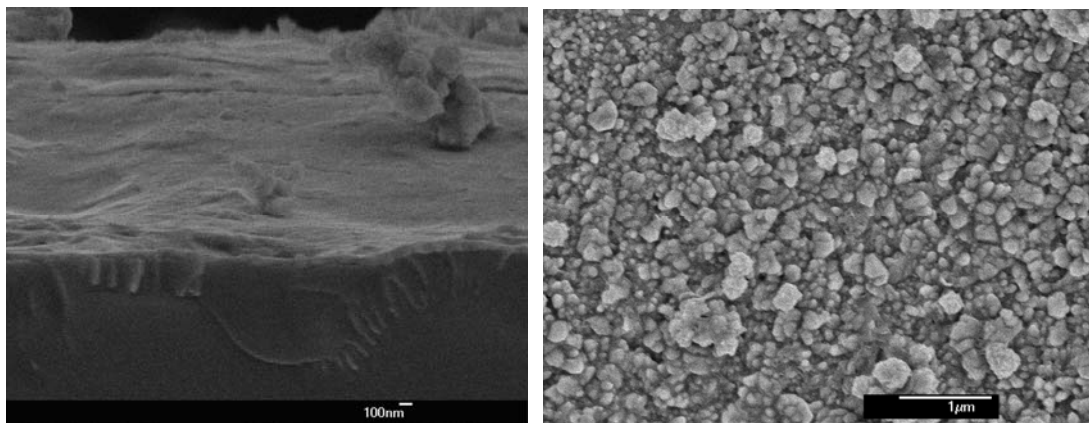
Figure 5.16   SEM images of CdS film (left) and CZTS nanoparticles [36] (right)

5.4.2   Future application - hybrid nanorod-polymer solar cells

Beside using all-oxide active layers for solar cell applications, hybrid nanorod-polymer solar cells also are good candidate for photovoltaic applications. These hybrid nanorod-polymer solar cells use a combination of a conjugated polymer and inorganic semiconductor nanorods to convert sunlight into electric charges.[14, 37, 38] The use of two materials with complementary p and n type electronic properties is crucial to the operation of the solar cell because photoexcitation of a conjugated polymer provides a bound electron-hole pair (exciton) rather than free charges. This exciton can be dissociated efficiently at the interface with a second material via a hole or electron transfer to produce the free charges that generate photovoltaic current. A complication arises because the exciton in conjugated polymers has a short lifetime (often sub-nanosecond) thus a correspondingly small (5-10 nm) diffusion range. Therefore, many polymer solar cells are designed to have a large area interface at short (nanometre) distances from anywhere within two materials by using a bulk heterojunction in which the two materials are mixed on a nanometre scale.

A second prerequisite for an efficient photovoltaic device is that both the p and n type material have continuous percolation pathways to transport the photogenerated holes and electrons to the electrodes. Although intimate mixing and co-continuous percolation may seem difficult to realize simultaneously, efficient bulk heterojunction

photovoltaic devices have been reported using polymer fullerene blends.

Compared to the organic solar cells, the hybrid solar cells have the advantage of being morphologically more stable and being able to utilize the high charge carrier mobility of the inorganic material. The challenge for the hybrid solar cells remains to create a morphology in which the inorganic and polymeric materials are intimately mixed on a nanometre scale but with co-continuous phases.[54]

One-dimensional (1D) inorganic semiconductor nanostructures provide a direct path for charge transport. Other advantages include high carrier motilities, solution processability, thermal and ambient stability, and a high electron affinity necessary for charge injection from the complementary organic donor material. ZnO nanorods are a typical example of this class of materials that have been used for hybrid solar cells.[55]

Hence, photogenerated hole or electron can transfer to produce the free charges in the contacts by the existence of the ZnO nanorods. Moreover, vertical alignment of ZnO nanorods is preferable because the structure provides a direct path of unique direction for charge transport so that the electron and hole motilities can be enhanced.

5.5 Conclusion

Vertical-aligned arrays of ZnO nanorod were grown on PET sheet, Ni-coated PET fibres and ZnO seed layer/Ni-coated PET fibres. The Ni-coated fibres with good

electrical conductivity to act as bottom electrode were fabricated by modified electroless Ni plating technique, while the n-type ZnO nanorods were deposited on the surface of PET sheet and Ni-coated polyester fibers using chemical solution deposition technique.

Structural and optical properties of the ZnO nanorods were characterized in details. For the structural characterization, sample A with ZnO nanorods of $1\,\mu$m in length and 300 nm in diameter and sample B with ZnO nanorods of $2\,\mu$m in length and 500 nm in diameter were deposited on top of about 150 nm-thick Ni layer coated on the PET fibres. ZnO nanorods with similar aspect ratio were obtained using different deposition times. Moreover, size and aspect ratio of the ZnO nanorods were not affected very much by different substrates. However, growth density of the ZnO nanorods was strongly influenced by different substrates. Ni layer seemed to assist the growth of ZnO nanorods, resulting in a more uniform and evenly distributed ZnO nanorod arrays on the PET surface. Moreover, the introduction of thin ZnO seed layer, derived from technique, between Ni layer and ZnO nanorod layer achieved denser and more uniform-distributed array but slower growth rate of the ZnO nanorods with a more vertical orientation.

Based on the XRD results, dominating diffraction peak of the nanorods on Ni-coated PET sheet was occurred at lattice plane (002). Highly c-axis oriented

crystalline nanorods were obtained on Ni-coated PET sheets. Besides, the XRD patterns with the supplementary Raman spectra indicated that the high-quality ZnO nanorods were grown on the Ni-coated PET sheets as well as the Ni-coated fibres.

The formation of large cracks in the Ni coating layer limited the application of the flexible electrode under high temperature conditions. This was probably due to large mismatch of the thermal coefficient of the Ni layer and the PET fibre substrate.

For the optical characterization results, the obtained bandgap energy of the ZnO nanorods was 3.95 eV which was larger than the reported bulk value of ZnO (3.37 eV). The difference in the bandgap values was possibly due to the influence of the voids in the ZnO nanorod array. Besides, low-transmittance ZnO nanorods had decreasing optical transmittance with increasing deposition time which was due to the longer nanorods as well as a denser packing obtained in the sample with longer deposition time.

Moreover, the vertically aligned ZnO nanorods were excited from ultraviolet laser source of λ=266 nm and released emission at λ=383 nm. Similar full-width at half-maximun (FWHM) of about 16 nm was obtained. Similar emission and linewidth were obtained from the ZnO nanorods of different deposition times. Hence, photoluminescence of the ZnO nanorods was independent of size of the nanostructure.

For the PV applications, thin film p-CZTS/i-CdS/n-ZnO junction solar cell has

been fabricated. The XRD and SEM results indicated that ZnO layer, CdS buffer layer

and CZTS nanoparticles were successfully fabricated separately.

CHAPTER 6 CONCLUSION

6.1 Metal coatings on PET sheets and fibres

Metal coatings of Au, Ni and Cu on 2D planar PET sheets and metal coatings of Ni and Cu on 3D circular PET fibres acting as the bottom electrodes of the flexible solar cells were successfully fabricated via a wet chemical techniques for metallization. In case of the metal coatings on the PET fibres, a technique modification was required. Two ends of the PET fibres were needed to thermally bonded onto the PET sheet and then dipped into chemical baths together for the metallization.

The electrodes were conductive, adhesive and flexible. In the application of organic solar cells, the Ni or Au coating has more appropriate work function to be the flexible electrodes of organic solar cells, comparing with Cu coating.

The four-point probe measurement verified that the metal layes were ohmic conductors. The ascending order of conductivity for the flexible electrodes was found to be Ni, Au and Cu. Besides, the crystal structure of the metal coatings was of single phase.

On the basis of our results, metallization condition to achieve Ni-coated PET fibres with good surface morphology as well as high conductivity was that the samples were etched with 4M NaOH solution at room temperature for two hours and the treated

samples were immediately dipped in the successive Pd-activation and Ni-plating baths

for six and three minutes respectively.

6.2 ZnO nanorod arrays grown on Ni-coated PET fibres

Vertical-aligned arrays of ZnO nanorod were grown on surface of the Ni-coated

PET fibres using chemical solution deposition technique.

Structurally, the sample of one-hour deposition time was $1\,\mu$m in length and 300

nm in diameter, while sample of three-hour deposition time was $2\,\mu$m in length and

500 nm in diameter. Both of them were deposited on top of 150 nm-thick Ni layer

coated on the PET fibres. Similar aspect ratio of the ZnO nanorods was obtained with

different deposition time. Moreover, growth density of the ZnO nanorods varied

largely in different substrates. Thin ZnO seed layer, derived from pulsed laser

deposition technique, was introduced between the Ni layer and the ZnO nanorods

achieved denser and more uniform-distributed alignment of the vertically aligned ZnO

nanorod arrays.

The dominating diffraction of the samples was occurred at ZnO(002) peaks

indicating highly vertical-aligned nanorods were grown on the Ni-coated PET sheets.

Besides, the XRD patterns with the supplementary Raman spectra shown that the

high-quality ZnO nanorods were grown on the Ni-coated PET sheets as well as the

fibres. However, formation of the large cracks on the Ni layer at higher temperatures limited the application of the flexible electrodes.

Optically, the bandgap value of the ZnO nanorods was 3.95 eV and the transmittance was low in visible spectrum. The transmittance also decreased with increasing deposition time. Moreover, the vertically aligned ZnO nanorods of different deposition times was excited at laser source of λ=266 nm and released edge-emission of λ=383 nm. Full-width at half-maximun of about 16 nm was obtained. According to our results, photoluminescence of the ZnO nanorods was independent of size of the nanostructure.

6.3 Future development of the flexible electrodes

The metal-coated polyester fibres of good conduction and flexibility were mainly designed and fabricated for the application of flexible solar cells integrated into clothing, in other words, "wearable solar cell".

The metalized PET sheets as well as fibres can be acted as bottom electrodes of organic solar cells and hybrid nanorod-organic hybrid solar cells, whereas the ZnO vertical-aligned nanorod arrays can be served as n-type material of the hybrid nanorod-organic solar cell on the polyester fibres.

Besides, the XRD and SEM results indicated that ZnO layer, CdS buffer layer and

CZTS nanoparticles were successfully fabricated separately. Thin film CIGS-like p-CZTS/i-CdS/n-ZnO junction solar cell on ITO glass substrate has been fabricated but failed to obtain I-V characteristic. Further junction improvements are needed to achieve successful I-V characteristic, in other words, solar cell performance. Eventually, the thin film solar cell on ITO glass substrate will be applied on flexible PET substrate coated with ITO.

APPENDIX A

| Pattern : 00-004-0836 | | Radiation = 1.540598 | | Quality : High |

Cu

Copper
Copper, syn

2th	i	h	k	l
43.298	100	1	1	1
50.434	46	2	0	0
74.132	20	2	2	0
89.934	17	3	1	1
95.143	5	2	2	2
116.923	3	4	0	0
136.514	9	3	3	1
144.723	8	4	2	0

Lattice : Face-centered cubic

S.G. : Fm-3m (225)

a = 3.61500

Mol. weight = 63.55

Volume [CD] = 47.24

Dx = 8.935

Dm = 8.950

Z = 4

Melting point: 1083°
Sample preparation: It had been heated in an H2 atmosphere at 300 C.
Sample source or locality: Sample from metallurgical laboratory of NBS, Gaithersburg, MD, USA.
Temperature of data collection: Pattern taken at 26 C.
General comments: Impurities from 0.001-0.01%, Ag, Al, Bi, Fe, Si, Zn.
Reflectance: Opaque mineral optical data on specimen from unspecified locality, $R_3R\%=60.65$, Disp.=Std.
Vickers hardness number: $VHN_{100}=96-104$,
General comments: Measured density and color from *Dana's System of Mineralogy, 7th Ed.,* I 99.
Color: Red
Additional pattern: See ICSD 64699 (PDF 85-1326).
Data collection flag: Ambient.

Swanson, Tatge., Natl. Bur. Stand. (U.S.), Circ. 539, volume I, page 15 (1953)

CAS Number: 7440-50-8

Radiation : CuKa1

Lambda : 1.54050

SS/FOM : F8= 89(0.0112,8)

Filter : Beta

d-sp : Not given

APPENDIX   B

Pattern : 00-036-1451		Radiation = 1.540598			Quality : High

ZnO

Zinc Oxide
Zincite, syn
Also called: chinese white, zinc white

2th	i	h	k	l
31.770	57	1	0	0
34.422	44	0	0	2
36.253	100	1	0	1
47.539	23	1	0	2
56.603	32	1	1	0
62.864	29	1	0	3
66.380	4	2	0	0
67.963	23	1	1	2
69.100	11	2	0	1
72.562	2	0	0	4
76.955	4	2	0	2
81.370	1	1	0	4
89.607	7	2	0	3
92.784	3	2	1	0
95.304	6	2	1	1
98.613	4	1	1	4
102.946	2	2	1	2
104.134	5	1	0	5
107.430	1	2	0	4
110.392	3	3	0	0
116.279	8	2	1	3
121.572	4	3	0	2
125.188	1	0	0	6
133.932	3	2	0	5
136.520	1	1	0	6
138.513	2	2	1	4
142.918	3	2	2	0

Lattice : Hexagonal	**Mol. weight =** 81.38
S.G. : P63mc (186)	**Volume [CD] =** 47.62
a = 3.24982	**Dx =** 5.675
c = 5.20661 **Z =** 2	

Sample source or locality: The sample was obtained from the New Jersey Zinc Co., Bethlehem, PA, USA.
Color: Colorless
General comments: The structure was determined by Bragg (1) and refined by Abrahams, Bernstein (2).
Polymorphism: A high pressure cubic NaCl-type of ZnO is reported by Bates et al. (3) and a cubic, sphalerite type is reported by Radczewski, Schicht (4).
Temperature of data collection: The approximate temperature of data collection was 26 C.
Additional pattern: To replace 5-664 (5).
Powder data (additional reference): References to other early patterns may be found in reference (5).
Optical data: B=2.013, Q=2.029, Sign=+
Data collection flag: Ambient.

McMurdie, H., Morris, M., Evans, E., Paretzkin, B., Wong-Ng, W., Ettlinger, L., Hubbard, C., Powder Diffraction, volume 1, page 76 (1986)

CAS Number: 1314-13-2

Radiation : CuKa1	**Filter :** Monochromator crystal
Lambda : 1.54060	**d-sp :** Diffractometer
SS/FOM : F27=131(0.0071,29)	

REFERENCES

[1] R.L. Crabb and F.C. Treble, "Thin silicon solar cells for large flexible arrays," *Nature*, vol. 214, pp. 1223–1224, 1967.

[2] M.A. Green, "Third generation photovoltaics: solar cells for 2020 and beyond," *Physica E*, vol. 14, pp. 65-70, 2002.

[3] N. Park, W. Kim and J. Kim, "Copper metallization of PET fabrics via intermediate polyaniline layers," *Fabrics and Polymers*, vol. 10, pp.310-314, 2009.

[4] B. Weintraub, Y. Wei and Z.L. Wang, "Optical fiber/nanowire hybrid structures for efficient three-dimensional dye-sensitized solar cells," *Angewandte Chemie International Edition*, vol. 48, pp.1-6, 2009.

[5] Michael R. Lee, Russell A. Gaudiana, et al., "Solar power wires based on organic photovoltaic materials," *Science*, vol.324, pp.232-235, 2009

[6] Y. Li, D. L. Carroll, et al., "The optics of organic photovoltaics: fiber-based devices," *IEEE Journal of Selected Topics in Quantum Electronics*, vol. 16, pp.1827-1837, 2010

[7] I.C. Cheng and S. Wagner, "Overview of flexible electronics technology," in *Electronic Materials: Science and Technology*, W.S.Wong and A. Salleo, Ed.

Germany: Springer, 2009, pp. 3-8.

[8] Y. H. Zhou, F. L. Zhang, et al., "Investigation on polymer anode design for flexible polymer solar cells," *Applied Physics Letters*, vol. 92, pp. 233308-233310, 2008.

[9] S. K. Hau, H. L. Yip, et al., "Indium tin oxide-free semi-transparent inverted polymer solar cells using conducting polymer as both bottom and top electrodes," *Organic Electronics*, vol. 10, pp. 1401-1407, 2009.

[10] S. Logothetidis and A. laskarakis, "Organic against inorganic electrodes grown onto polymer substrates for flexible organic electronics applications," *Thin Solid Films*, vol.518, pp. 1245-1249, 2009.

[11] F. Yang and S. R. Forrest, "Organic solar cells using transparent SnO_2-F anodes," *Advanced Materials*, vol. 18, pp. 2018-2022, 2006.

[12] A. D. Pasquier, M. Stewart, et al., "Aqueous coating of efficient flexible TiO_2 dye solar cell photoanodes," *Solar Energy Materials and Solar Cells*, vol. 93, pp. 528-535, 2009.

[13] M. W. Rowell, M. A. Topinka, et al., "Organic solar cells with carbon nanotube network electrodes," *Applied Physics Letters*, vol. 88, pp. 233506-233508, 2006.

[14] Z. Wu, Z. Chen, et al., "Transparent, conductive carbon nanotube films," *Science*, vol. 305, pp. 1273-1276, 2004.

[15] V. Scardaci, R. Coull and J. N. Coleman, "Very thin transparent, conductive

carbon nanotube films on flexible substrates," *Applied Physics Letters*, vol. 97, pp. 023114-023116, 2010.

[16] G. Eda, G. Fanchini and M. Chhowalla, "Large-area ultrathin films of reduced grapheme oxide as a transparent and flexible electronic material," *Nature Nanotechnology*, vol. 3, pp. 270-274, 2008.

[17] X.Wang, L. Zhi, et al., "Transparent carbon films as electrodes in organic solar cells," *Angewandte Chemie International Edition*, vol. 47, pp. 2990-2992, 2008.

[18] M. J. Allen,V. C. Tung, et al., "Soft transfer printing of chemically converted graphene," *Advanced Materials*, vol. 21, pp. 2098-2102, 2009.

[19] S. K.Hau, H. L. Yip, et al., "Spraycoating of silver nanoparticle electrodes for inverted polymer solar cells," *Organic Electronics*, vol. 10, pp. 719-723, 2009.

[20] W. Gaynor, J. Y. Lee and P. Peumans, "Fully solution-processed inverted polymer solar cells with laminated nanowire electrodes," *ACS Nano*, vol. 4, pp. 30-34, 2010.

[21] Industrial Centre Technical Staff, *Surface Finishing,* Industrial Centre of The HK Polytechnic University, 2011.

[22] F. Garbassi, M. Morra, et al., *Polymer Surface: from Physics to Technology*, England: Wiley, 1998.

[23] C.S. Ng, "Metallization of engineering plastics," M.S. thesis, The HK

Polytechnic University, Hong Kong, China, 2009.

[24] READE Advanced Materials, USA, "Metallizing Powders And Metallizing Wires," 2011, http://www.reade.com/products/121-metallizing-compounds/561.

[25] Jenny Nelson, "Organic and plastic solar cells," in *Practical Handbook of Photovoltaics: Fundamentals and Applications*. T. Markvart and L. Castaner, Ed. New York : Elsevier Advanced Technology, 2003, pp.484-488.

[26] S.H. Jin, B.V.K. Naidu, et al., "Optimization of process parameters for high-efficiency polymer photovoltaic devices based on P3HT:PCBM system," *Solar Energy Materials and Solar Cells*, vol. 91, pp.1187-1193, 2007.

[27] Wendy U. Huynh, Janke J. Dittmer and A. Paul Alivisatos, "Hybrid nanorod-polymer solar cells," *Science*, vol. 295, pp.2425-2427, 2002.

[28] S. T. Tan, B. J. Chen, et al., "Blueshift of optical band gap in ZnO thin films grown by metal-organic chemical-vapor deposition," *Journal of Applied Physics*, vol. 98, pp. 013505-013505-5, 2005.

[29] R.K. Khanna, "Raman-spectroscopy of oligomeric SiO species isolated in solid methane," *Journal of Chemical Physics*, vol. 74, pp.2108-2115, 1981.

[30] S.M. Sze, *Semiconductor Devices, Physics and Technology*. New York: Wiley, 1985, pp34-38.

[31] "Optical transmittance measurements and bandgap energy," teaching module for

Display Materials Lab, Department of Materials Science and Engineering, Korea Advanced Institute of Science and Technology, 2010.

[32] M. Al-Ibrahim, H.K. Roth, et al., "The influence of the optoelectronic P3HT on the device parameters in flexible polymer solar cells," *Organic Electronics*, vol. 6, pp.65-77, 2005.

[33] H.B. Michaelson, "The work function of the elements and its periodicity," *Journal of applied physics*, vol. 14, pp.4729-4733, 1977.

[34] V. Shrotriya, Y. Yang, et al., "Absorption spectra modification in poly(3-hexylthiophene):methanofullerene blend thin films", *Chemical Physics Letters*, vol. 411, pp138-143, 2005

[35] M. Al-Ibrahim, S. Sensfuss, et al., "The influence of the optoelectronic properties of poly(3-alkylthiophenes) on the device parameters in flexible polymer solar cells," *Organic Electronics*, vol. 6, pp. 65-77, 2005

[36] C. Lungenschmied, G. Dennler, et al., "Flexible, long-lived, large-area, organic solar cells," *Solar energy materials and solar cells*, vol. 91, pp.379-384, 2007

[37] R. Serway, *Principles of Physics* (2nd ed.). London: Saunders College Pub, 1998, p602.

[38] D. Griffiths, *Introduction to Electrodynamics* (3rd ed.). New Jersey: Prentice Hall, 1999, p286.

[39] Cable Solutions Group, Teledyne Storm Products, Inc. at Dallas, USA, "Room-temperature linear coefficient of thermal expansion values for various engineering materials," 2010,

http://www.stormcable.com/uploads/Thermal_expansion_data_table_tb06.pdf

[40] C.H. Xue, R.L. Wang, et al., "Growth of ZnO nanorod forests and characterization of ZnO-coated nylon fibers," *Materials Letters*, vol. 64, pp. 327-330, 2010.

[41] R.H. Wang, J.H. Xin, et al., "ZnO Nanorods grown on cotton fabrics at low temperature," *Chemical Physics Letters*, vol. 398, pp. 250-255, 2004.

[42] B. Xu and Z.S. Cai, "Fabrication of a superhydrophobic ZnO nanorod array film on cotton fabrics via a wet chemical route and hydrophobic modification," *Applied Surface Science*, vol. 254, pp. 5899-5904, 2008.

[43] M. Law, L.E. Green, et al., "Nanowire dye-sensitized solar cells," *Nature Materials*, vol. 4, pp. 455-459, 2005.

[44] L.E. Greene, B.D. Yuhas, et al., "Solution-growth zinc oxide nanowires," *Inorganic Chemistry*, vol. 45, pp. 7535-7544, 2006.

[45] J.B. Cui, C.P. Daghlian, et al., "Low-temperature growth and field emission of ZnO nanowire arrays," *Journal of Applied Physics*, vol. 97, pp. 44315/1-44315/7, 2005.

[46] L. Liao, D.H. Liu, et al., "Synthesis and Raman analysis of 1D-ZnO nanostructure via vapor phase growth," *Applied Surface Science*, vol. 240, pp. 175-179, 2005.

[47] V. Yu. Davydov, Yu. E. Kitaev, et al., "Phonon dispersion and Raman scattering in hexagonal GaN and AlN," *Physical Review B*, vol. 58, pp. 12899-12907, 1998.

[48] Y. Gu, Igor L. Kuskovsky, et al. "Quantum confinement in ZnO nanorods," *Applied Physics Letters*, vol. 85, pp. 3833-3835, 2004.

[49] Eunice S.P. Leong, S.F. Yu, et al., "Edge-emitting vertically aligned ZnO nanorods random laser on plastic substrate," *IEEE Photonic Technology Letters*, vol. 10, pp. 1792-1794, 2007.

[50] C. Steinhagen, M.G. Panthani, et al., "Synthesis of Cu2ZnSnS4 nanocrystals for use in low-cost photovoltaics," *Journal of the American Chemical Society*, vol. 131, pp. 12554-12555, 2009.

[51] R. Naciri, H. Bihri, et al., "The role of the CdS buffer layer in the CuInS2 Thin film solar cell," *Revue des Energies Renouvelables CER'07 Oujda*, pp. 165-168, 2007.

[52] A.E. Rakhshani and A.S. Al-Azab, "Characterization of CdS films prepared by chemical-bath deposition," *Journal of Physics: Condensed Matter*, vol. 12, pp. 8745-8755, 2000.

[53] W.C. Liu (private communication), 2011.

[54] W. Beek, M. Wienk and R. Janssen, "Hybrid polymer solar cells based on zinc oxide," *Journal of Materials Chemistry*, vol. 15, pp. 2985-2988, 2005.

[55] Alejandro L. Briseno, Thomas W. Holcombe, et al., "Oligo~ and polythiophene/ZnO hybrid nanowire solar cells," *Nano Letters*, vol. 10, pp. 334-340, 2010.